HLA antibody affinity determination: from HLA-specific monoclonal antibodies to donor HLA specific antibodies (DSA) in patient serum

Hug, M.N.; Keller, S.; Marty, T.; Gygax, D.; Meinel, D.; Spies, P.; ... ; Honger, G.

Note: To cite this publication please use the final published version (if applicable).

ORIGINAL ARTICLE

HLA antibody affinity determination: From HLA-specific monoclonal antibodies to donor HLA specific antibodies (DSA) in patient serum

Melanie N. Hug[1#] | Sabrina Keller[1#] | Talea Marty[1] | Daniel Gygax[1] |
Dominik Meinel[1] | Peter Spies[1] | Joëlle Handschin[2] | Marc Kleiser[3] |
Noemi Vazquez[2] | Janina Linnik[2,4,5] | Rico Buchli[6] | Frans Claas[7] |
Sebastiaan Heidt[7] | Cynthia S. M. Kramer[7] | Suzanne Bezstarosti[7] |
Jar-How Lee[8] | Stefan Schaub[2,3,9] | Gideon Hönger[2,3]

[1]University of Applied Sciences and Arts Northwestern Switzerland, School of Life Sciences Muttenz, Muttenz, Switzerland

[2]Department of Biomedicine, University of Basel, Basel, Switzerland

[3]Department of Laboratory Medicine, University Hospital Basel, Basel, Switzerland

[4]Department of Biosystems Science and Engineering, ETH Zurich, Basel, Switzerland

[5]Swiss Institute for Bioinformatics, Basel, Switzerland

[6]Department of Research and Development, PureProtein LLC, Oklahoma City, Oklahoma, USA

[7]Department of Immunology, Leiden University Medical Center, Leiden, The Netherlands

[8]Research Department, Terasaki Innovation Center (TIC), Glendale, California, USA

[9]Clinic for Transplantation Immunology and Nephrology, University Hospital Basel, Basel, Switzerland

Correspondence
Gideon Hönger, Department of Biomedicine, University of Basel, Basel, Switzerland.
Email: gideon.hoenger@usb.ch

Organs transplanted across donor-specific HLA antibodies (DSA) are associated with a variety of clinical outcomes, including a high risk of acute kidney graft rejection. Unfortunately, the currently available assays to determine DSA characteristics are insufficient to clearly discriminate between potentially harmless and harmful DSA. To further explore the hazard potential of DSA, their concentration and binding strength to their natural target, using soluble HLA, may be informative. There are currently a number of biophysical technologies available that allow the assessment of antibody binding strength. However, these methods require prior knowledge of antibody concentrations. Our objective within this study was to develop a novel approach that combines the determination of DSA-affinity as well as DSA-concentration for patient sample evaluation within one assay. We initially tested the reproducibility of previously reported affinities of human HLA-specific monoclonal antibodies and assessed the technology-specific precision of the obtained results on multiple platforms, including surface plasmon resonance (SPR), bio-layer

---

[#] Shared first authorship.

interferometry (BLI), Luminex (single antigen beads; SAB), and flow-induced dispersion analysis (FIDA). While the first three (solid-phase) technologies revealed comparable high binding-strengths, suggesting measurement of avidity, the latter (in-solution) approach revealed slightly lower binding-strengths, presumably indicating measurement of affinity. We believe that our newly developed in-solution FIDA-assay is particularly suitable to provide useful clinical information by not just measuring DSA-affinities in patient serum samples but simultaneously delivering a particular DSA-concentration. Here, we investigated DSA from 20 pre-transplant patients, all of whom showed negative CDC-crossmatch results with donor cells and SAB signals ranging between 571 and 14899 mean fluorescence intensity (MFI). DSA-concentrations were found in the range between 11.2 and 1223 nM (median 81.1 nM), and their measured affinities fall between 0.055 and 24.7 nM (median 5.34 nM; 449-fold difference). In 13 of 20 sera (65%), DSA accounted for more than 0.1% of total serum antibodies, and 4/20 sera (20%) revealed a proportion of DSA even higher than 1%. To conclude, this study strengthens the presumption that pre-transplant patient DSA consists of various concentrations and different net affinities. Validation of these results in a larger patient cohort with clinical outcomes will be essential in a further step to assess the clinical relevance of DSA-concentration and DSA-affinity.

1 | INTRODUCTION

Donor-specific antibodies (DSA) are associated with clinical and subclinical antibody-mediated rejection (AMR) and allograft loss,[1–4] caused by their main effector functions such as HLA crosslinking triggering endothelial activation,[5] C1q-binding leading to complement activation[6–8] and FcγR-binding inducing cellular cytotoxicity.[8–11] However, a substantial proportion of DSA-positive recipients experience an uneventful and rejection-free course.[1,12–15] Much research has been carried out aiming to identify DSA features that predict their clinical relevance. It was found that neither the route of sensitization (blood-transfusions, pregnancies, previous transplantations)[16] nor the five readily available pre-transplant DSA characteristics (DSA number, DSA HLA-class specificity, DSA HLA locus specificity and cumulative DSA test signal strength, DSA titer), outputs of the gold-standard assay to characterize DSA (Single Antigen Bead assay; SAB), are sufficient to distinguish between potentially harmless DSA and DSA with detrimental effects.[1,17–19] However, it has been shown that C1q binding DSA, i.e. DSA of IgG1 and IgG3 antibody subclasses, are clearly

associated with rejection,[20] but the breakdown of pre-Tx HLA antibody mixtures has also revealed that the vast majority of pre-transplant HLA antibodies are mixtures containing at least one of these complement binding subclasses.[21,22]

Validation parameters beyond the mentioned basic DSA characteristics, including DSA binding strength, potentially provide better information in predicting the pathogenic potential of circulating DSA. However, clinically validated methods for assessing the binding strength of DSA in transplant patient sera have not yet been implemented.

Depending on the spatial proximity of antigenic repetitive structures on the same antigen or critical binding sites on closely spaced antigens, one or more fragments of antigen binding (Fab) domains of antibodies may bind, resulting in a measurable difference in binding strength. Generally, the resulting binding of the former situation is called "affinity", while the latter situation (i.e. both Fab involved for IgG) results in stronger binding and is termed "avidity". Regardless of whether the methods used in this study preferably measured "affinity" or "avidity", we use the term "affinity" throughout the text of this publication for simplicity.

Generally, binding affinity is a measure of how strongly two molecules can interact with each other and is reported by the dissociation equilibrium constant (K_D; [M]). The K_D-value of an antibody represents the antibody concentration at which half of the antibody binding sites on the antigen are occupied at the equilibrium of the paratope-epitope binding reaction. One way to measure antibody affinity is real-time interaction analysis, where the rate of complex formation is measured from which the K_D can be determined directly upon dividing the dissociation rate constant (k_d; [1 s^{-1}]) by the association rate constant (k_a; [1/Ms]).[23] The second way is a measurement after the binding reaction has reached the equilibrium (end-point measurement) and needs a titration of either the antigen or the antibody, expressed through a dose–response model. By using the inflection point of the given sigmoidal antibody–antigen binding curve, half maximum binding concentration can be assessed in order to indirectly measure antibody affinity. Importantly, every antibody affinity determination approach requires knowledge of the antibody concentration (i.e. mAb) or its simultaneous determination.

To date, several biophysical methods have been used for determination of HLA-antibody affinity: Surface Plasmon Resonance (SPR),[24–27] Bio-Layer Interferometry (BLI),[28,29] Microfluidic Diffusional Sizing (MDS)/Microfluidic Antibody Affinity Profiling (MAAP)[29,30] and SAB assays.[26,31] Their main characteristics are summarized in Table 1. However, the few publications mainly provide data on HLA-specific monoclonal antibodies (mAbs).[26,27,29] Determination of HLA antibody affinity in patient serum is more challenging. While Visentin et al. spiked HLA-specific mAbs into negative control serum to mimic the usual matrix for their SPR experiments,[27] Schneider et al. applied real patient serum samples for their MAAP measurements but only provided affinity values from four allo-antibodies.[29]

Immobilization-free ligand binding technologies for in-solution analysis of size, quantity and binding properties of pre-labeled fluorescent biomolecules offer several advantages for antibody affinity determination, especially for complex matrices such as patient serum. Some of the benefits of these assays are a better control of antigen concentration and antigen accessibility, a relatively short experimental hands-on time, and comparatively low costs. In addition, the technology is less susceptible to interferences such as rebinding effects or high-dose hook effect. Furthermore, serum samples do not have to be pre-treated as the method is less vulnerable to complement-interference known to cause false-negative results in solid-phase binding assays such as SAB.[32,33] Particularly noteworthy are two methodologies/platforms that characterize antibody–antigen binding using the

TABLE 1 Characteristics of applied binding technologies

Technology/platform	Abbreviation	Assay type	Modification of one of the molecular binding partners	Flow	K_D determination	Sensitivity
Surface Plasmon Resonance	SPR	solid-phase assay	e.g. biotinylation	yes (fluidic flow)	real time interaction analysis; determination of k_a and k_d	k_a: 10^3 to 10^7 M^{-1} s^{-1} k_d: 10^{-1} to 5×10^{-6} s^{-1} K_D: 1×10^{-4} to 2×10^{-10} M
Bio-Layer Interferometry	BLI	solid-phase assay	e.g. biotinylation	no (closed cavity)	real time interaction analysis; determination of k_a and k_d	k_a: 10^1 to 10^7 M^{-1} s^{-1} k_d: 10^{-1} to 10^{-6} s^{-1} K_D: 1×10^{-3} to 1×10^{-11} M
Luminex Single Antigen Beads	SAB	solid-phase assay	n/a	no (closed cavity)	steady state affinity; determination of half maximum binding	K_D: 1×10^{-8} to 1×10^{-11} M
Flow Induced Dispersion Analysis	FIDA	immobilization-free (in solution assay)	fluorescent labeling	yes (thin capillary)	steady state affinity; determination of half maximum binding	K_D: 1×10^{-7} to 1×10^{-11} M
Microfluidic Diffusional Sizing (MDS)	MDS	immobilization-free (in solution assay)	fluorescent labeling	yes (microfluidic system)	steady state affinity; determination of half maximum binding	K_D: 1×10^{-7} to 1×10^{-11} M

approach described above: MDS[34]/MAAP)[29,30] and Flow-induced dispersion analysis (FIDA).[35] In this study, we used the latter technology/platform to determine HLA antibody affinity. The ligand (here fluorescently labeled soluble HLA) is first pre-mixed and incubated with titrated analyte (here HLA-specific mAb or patient serum containing DSA), and the mixture is then injected into a thin capillary to monitor (e.g. using a fluorescence detector) the diffusion behavior of the present molecule mixture under a laminar flow. The more antigen–antibody complexes formed, the higher the diffusion, the slower their movement in the capillary, the broader the resulting fluorescence peak. Subsequent analysis of the fluorescence peak reveals the average hydrodynamic radius of present molecules/molecule-complexes and can be plotted against concentration or serum fraction, in order to assess half-maximum binding, used to determine antibody-affinity.

The aim of this study was to develop an approach that concurrently resolves DSA-concentration and DSA-affinity in patient serum samples, and to subsequently evaluate the two measures in a set of well-characterized pre-transplant DSA-containing sera ($n = 20$).

In addition to the binding force between antibody and cognate antigen, the specifically targeted surface area on the antigen is of critical interest. In this context, we use the terms 'structural epitope' and 'functional epitope' throughout the manuscript. The former term refers to the entire three-dimensional surface area masked by the paratope of the antibody,[36] while the latter refers to the functionally crucial amino acids within this area, also termed 'eplet',[37] which mainly interact with the most hyper-variable region of the antibody, the complementarity-determining region 3 (CDR3).[38]

2 | MATERIALS AND METHODS

2.1 | Antigens

2.1.1 | Soluble HLA molecules

Soluble HLA (sHLA), used within this study for BLI-, SPR- and FIDA-experiments, were kindly provided by PureProtein LLC, Oklahoma City/OK/USA. Highly purified proteins were prepared according to techniques described previously.[39] In this study, we used either biotinylated (for BLI and SPR) or conjugated to AlexaFlour488 (for FIDA).

To assure antigenicity and HLA protein stability, each molecule was validated using subtype specific sandwich ELISA approaches. Individual molecules were titrated and experimental data plotted in semi-log plots with the x-axis representing the different dilutions in log scale and the y-axis showing the signal response data (OD_{490}) for each experimentally derived dilution. Curve parameters were determined by nonlinear curve fitting to a dose–response model with variable slope using the software package Prism (Graph Pad Software, Inc., San Diego, CA). Half maximum concentration (EC_{50}), Hill slope and R^2 values were reported.

2.1.2 | Single HLA beads

For all titration experiments performed by Luminex, we utilized HLA-coated single antigen beads (SAB) from ThermoFisher/OneLamda (West Hills/CA/USA).[40] To circumvent the 'shared-epitope-phenomenon',[41,42] we used individual bead sets (SAB_{mono}), representing a single HLA type only. For each SAB_{titr}-assay, we additionally used negative (uncoated) control beads (NCB). Both bead types, SAB and NCB, were kindly provided by ThermoFisher/OneLambda.

2.2 | Antibodies

2.2.1 | HLA-specific monoclonal reference antibodies

Human HLA-specific mAbs were kindly provided by the National Reference Centre (NRC) for Histocompatibility Research [Leiden, the Netherlands, (https://nrc-hla.nl/)]. They were derived from human hybridoma cells [Epstein–Barr virus (EBV) transformed B-lymphocytes of HLA antibody positive multiparous women sensitized during pregnancy]. Their characteristics are presented in Table 2. Upon receipt, the mAbs derived from hybridoma cell culture supernatants were purified and concentrated by using Pierce Protein Concentrators PES columns (100 K MWCO / 0.5 mL, #88503, ThermoFisherScientific/Waltham/MA/USA) and the final concentration of each mAb solution was assessed using the chemiluminescence based Mesoscale Discovery® (MSD) human immunoglobulin isotyping assay (K15203D, MSD/Rockville/MD/USA).

Additional reference antibodies were obtained from InvivoGen, San Diego/CA/USA (W6/32 and F3.3) or received as a gift from PureProtein LLC, Oklahoma City/OK/USA (L243 and Anti-Zipper Ab), and their specificity is described in Table 2.

2.2.2 | DSA positive serological specimen

To exemplarily demonstrate affinity measurement on relevant patient samples, 20 pre-transplant serum samples

TABLE 2 Characteristics of used HLA-specific monoclonal antibodies

mAb	host	Source	Publication	Isotype	serological HLA-specificity (by CDC) / notes	immunizer-HLA or -haplotype	tested with HLA-subtype(s)	targeted functional epitope (eplet)	critical position/AA*
SN230G6	human	NRC Leiden	J Immunol 2005; 175:5950–57	IgG1, Lambda	A2/B17	A2; B57	A*02:01 B*57:01	62GE	62G 63E
SN607D8	human	NRC Leiden	Front Immunol 2022:12:800946	IgG1, Kappa	A2/A28	A2; B57	A*02:01 B*68:01	144TKH	142T 144K 145H
SN66E3	human	NRC Leiden	Front Immunol 2022:12:800946	IgM, Kappa	A2/A28	A2; B57	A*02:01	145KHA	144K 145H 149A
BRO11F6	human	NRC Leiden	Hum Immunol 2013; 74:1271–1279	IgG1, Lambda	A11	unknown	A*01:01 A*11:01	unresolved	144K 145R 151H
WIM8E5	human	NRC Leiden	Transpl Int 2019; 32:16–24	IgG1, Kappa	A1/A10/A11/A9/ A29/A30/A31/ A33/A28	unknown	A*01:01 A*11:01	unresolved	HLA-A: 161E (109F); HLA-B: unknown; HLA-C: 173 K
MUL2C6	human	NRC Leiden	Transplantation 2004; 78:995–1001	IgG1, Lambda	A3/A11/A24	A11; B55; C3	A*11:01	144 KR	144K 145R
MUL4C8	human	NRC Leiden	Transplantation 2010; 90: 1468–72	IgG1, Kappa	A3/A11	A11; B55; C3	A*01:01 A*11:01	unresolved	142I 144K 145R
VIN1B10	human	NRC Leiden	no published reports	IgG1, Kappa	A1/A11/A26/A34	unknown	A*11:01	unresolved	
BOY2A7	human	NRC Leiden	no published reports	IgG1, Kappa	A10/A11	unknown	A*11:01	unresolved	
OUW4F11	human	NRC Leiden	Hum Immunol 2012; 73:267–277	IgG1, Lambda	Bw6	A1; B8; C7	B*07:02 B*08:01 B*35:01	80N	80 N
VTM1F11	human	NRC Leiden	Mol Immunol 2010; 47:809–815	IgG1, Kappa	B27/B7/B40/B48	A1; B7; C7	B*07:02 B*27:05	unresolved	163E
WK1D12	human	NRC Leiden	Transplantation 2010; 90:1468–72	IgG1, Kappa	B7/B27/B60	B27	B*07:02 B*27:05	unresolved	163E 76E(self)

TABLE 2 (Continued)

mAb	host	Source	Publication	Isotype	serological HLA-specificity (by CDC) / notes	immunizer-HLA or -haplotype	tested with HLA-subtype(s)	targeted functional epitope (eplet)	critical position/AA*
VTM4D9	human	NRC Leiden	Front Immunol 2022;12:800946	IgG1, Kappa	B7/B27/B55/B56	A1; B7; C7	$B*07:02$ $B*27:05$	65QIA	65Q 66I 69A
VTM9A10	human	NRC Leiden	Hum Immunol 2012; 73:267–277	IgG1, Kappa	B7/B27/B54/B55/ B56//B67/B82	A1; B7; C7	$B*07:02$ $B*27:05$	65QIA	65Q 66I 69A
reference mAb W6/32	(chimeric; human/ mouse)	InvivoGen	J Immunol Methods 2013; 390:41–51	IgG1, Kappa	anti HLA class I pan		$A*02:01$ $A*11:01$ $B*07:02$	(public conformational HLA-class I epitope)	$121K_{heavy\ chain}$ $3R_{b-2m}$
reference mAb F3.3	(chimeric; human/ mouse)	InvivoGen	J Immunol Methods 2013; 390:41–51	IgG1, Kappa	anti HLA-DR/ -DP/ partly -DQ		$DRB1*07:01$	unresolved	HLA-DR/ -DQ: $46E_{beta}$; HLA-DP: $44E_{beta}$
reference mAb L243	mouse	PureProtein	no published reports	IgG2a, Kappa	anti HLA-DR			unresolved	
reference mAb antiZIP	mouse	PureProtein	no published reports	IgG1, Kappa	anti Leucine Zipper; soluble HLA2-ZP			not HLA-specific, Leucine zipper structure specific	

Note: AA, amino acid; b-2 m, beta2-microglobulin; beta, beta-chain; CDC, complement dependent cytotoxicity.

were obtained from sensitized kidney recipients later transplanted across a single DSA per HLA-class. They were chosen upon the constrained availability of corresponding sHLA and SAB$_{mono}$ molecules. The specificity of these antibodies against HLA of the corresponding donor was assigned at the allelic level by the virtual-crossmatch-approach[43] for IgG, IgM and IgA (using the following reporter-antibody-R-PE-conjugates: anti-IgGpan: polyclonal goat-anti-human-IgG-, F(ab')₂, LS-AB2, OneLambda; anti-IgM: polyclonal donkey-anti-human-IgM, IgM-PEC1, OneLambda; anti-IgA1/IgA2: mouse-(IgG1)-anti-human-IgA1/2 Fc, clones B3506B4/A9604D2 and 9130–09/9140–09, Southern Biotec/Birmingham/AL/USA). IgG subclasses were determined using the following R-PE-conjugated subclass-specific reporter antibodies provided by Southern Biotec: anti-IgG1: #905409 clone HP6001, anti-IgG2: #907009 clone HP6002, anti-IgG3: #921009 clone HP6050, anti-IgG4: #920009 clone HP6025. DSA dependent C3d-binding was assessed using polyclonal anti-C3d-PE from Immucor (Norcross/GA/USA). DSA isotype-, IgG-subclass- and C3d-binding-characterization was realized using LabScreen SAB$_{multi}$ from OneLambda, using a Luminex LX-200 instrument. For the assignment of a positive result the arbitrary cutoff of 500 MFI was used for DSA$_{IgG}$, DSA$_{IgM}$ and DSA$_{IgA}$, while for DSA$_{IgG1/2/3/4}$, the biological cutoff (mean background signal of SAB$_{self-HLA}$ plus 3 standard deviations) was applied,[44] and the applied cutoff for C3d-positivity was the mean MFI signal of 4 negative control sera plus 3 standard deviations. To determine the specificity of investigated DSA towards antibody-verified eplets, donor/recipient high resolution HLA typing data and the corresponding HLA antibody binding pattern were analyzed using HLAMatchmaker v3.1. To calculate
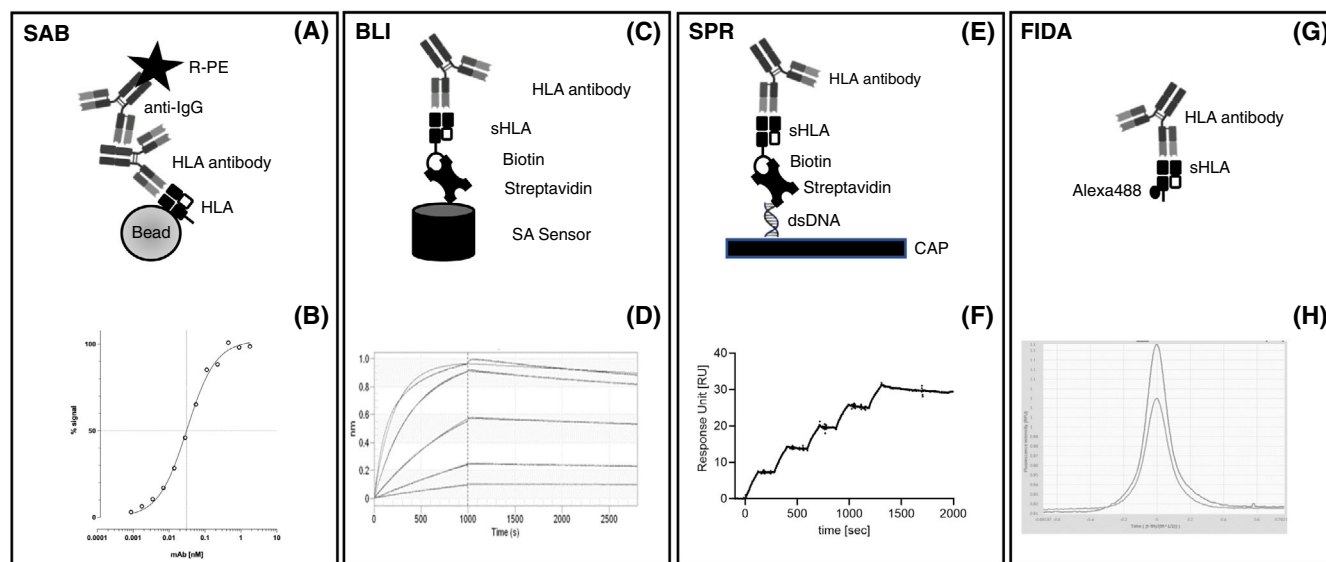

FIGURE 1   Experimental setup and result output of the four technologies used. (A) SAB assay experimental setup. HLA molecules coated onto polystyrene beads are incubated with different HLA antibody concentrations. Bound antibodies at steady state are recorded via the isotype-specific fluorochrome (R-PE) conjugated reporter antibody. (B) Percentage binding signal plotted against mAb concentration. 50% signal reveals the antibody concentration required to occupy half of the antibody-binding sites on the antigen (HLA) at equilibrium. (C) BLI assay experimental setup. Biotinylated sHLA bound via streptavidin-conjugated SA-sensors are incubated with HLA antibody solutions of different concentration. (D) The BLI sensorgram visualizes the binding interaction profile between immobilized HLA antigen and 6 different antibody concentrations over time and allows to determine the antibody on- and off-rate in real-time and thereby the disassociation equilibrium constant. (E) SPR assay experimental setup. Biotinylated sHLA bound via streptavidin-DNA to the CAP surface interacts with HLA antibodies at different concentrations. (F) The SPR sensorgram visualizes the binding interaction between immobilized HLA antigen and 5 different HLA antibody concentrations over time and allows to determine the antibody on- and off-rate in real-time and thereby the disassociation equilibrium constant. (G) FIDA assay experimental setup. In solution, soluble fluorochrome (AlexaFluor488)-labeled HLA molecules are incubated with different HLA antibody concentrations until equilibrium and thereafter each solution is injected into a thin capillary under a laminar flow. (H) Taylorgram of a FIDA experiment: Binding of antibodies is measured via complex size determination based on diffusivity change upon antigen–antibody complex formation. The broadness of the recorded fluorescence peek reveals the average hydrodynamic radius of present molecules/complexes and allows to generate a binding curve (further explained in document S1) from which half-maximal binding can be deduced. (Alexa488 = bright green fluorescence dye, BLI = Bio-Layer Interferometry, dsDNA = double-stranded DNA, FIDA = Flow-induced dispersion analysis, IgG = Immunoglobulin G, R-PE = R-Phycoerythrin, SAB = Single Antigen Beads, sHLA = soluble HLA, SPR = Surface Plasmon Resonance)

the fraction of circulating DSA within the total IgG present in the serum, we determined total serum IgG with the Luminex Immunoglobulin-Isotyping-Panel HGAMMAG-201 K from Millipore/Billerica/MA/USA. DSA characteristics are summarized in Table 4.

2.2.3 | Negative control serum

For experiments that included the spiking of sera with HLA-specific mAb, we used the LABScreen™ Negative Control Serum LS-NC from OneLambda, that consists of pooled, high speed centrifugated and filtered (0.25 μm) undiluted negative serum samples drawn from 5 to 10 non-transplanted and non-transfused male blood donors.

2.3 | Biophysical binding measurement platforms and technologies

We applied the four technologies described below to measure and cross-compare affinities of HLA-specific mAbs. To measure affinities of DSA from patient serum samples, we used the in-solution (i.e. immobilization-free) ligand binding technology FIDA exclusively.

2.3.1 | SAB$_{titr}$-assay

The setup of the SAB$_{titr}$-assay is visualized in Figure 1A. For each assay application, we applied 1000 beads. We adjusted the bead concentration using the handheld particle counting device Scepter 2.0 (Millipore, Billerica, Massachusetts, USA). We serially diluted the mAb of interest and tested at least eight mAb concentrations. All SAB$_{titr}$-assays were executed in a total volume of 15 μL (3 μL SAB solution containing 1000 SAB$_{mono}$, 2 μL NCB solution containing 1000 NCB and 10 μL mAb solution in phosphate-buffered saline (PBS) containing 1% bovine serum albumin (BSA)). The following incubation conditions were applied: 30 min, plates covered with aluminum foil to protect from light, rotation with 500 rpm on a IKA MS3 digital plate rotator (Guangzhou, China). After removing the supernatant and washing, the beads were incubated (using the same conditions as described above) with the isotype-specific R-PE-conjugated secondary antibody (concentration: 16 ng/mL) in a volume of 15 μL. After washing, we acquired and analyzed at least 100 beads on a Luminex 200 instrument and evaluated their R-PE-conjugate derived MFI signal. Trimmed MFI values of the NCB were subtracted from the trimmed MFI values of the analyzed SAB, revealing the final MFI result. Using the MFI value obtained for each titration point, we plotted a binding curve and applied nonlinear

regression curve fitting with the function "specific binding with Hill slope",

$$y = B_{max} {}^* x^h / (K_D{}^h + x^h)$$

(x = concentration; y = % signal; B$_{max}$ = maximum binding; K$_D$ = mAb concentration that binds to half of binding sites on HLA at equilibrium; h = Hill slope)

and calculated the maximum and subsequently half maximum binding signal. A typical SAB$_{titr}$ binding curve of an HLA-specific mAb, after normalization to % binding, is shown in Figure 1B.

2.3.2 | BLI-assay

BLI can detect label-free molecules in a fluidic-free environment. The method records the reflexion of white light from two surfaces: the surface layer on the (streptavidin coated) biosensor tip with the immobilized protein (here biotinylated sHLA) and an internal reference layer. Molecules binding to or dissociating from the biosensor (here HLA antibodies) shift the interference pattern and generate a response profile (nm-shift).

The setup of the BLI-assay is visualized in Figure 1C. We first immobilized biotinylated sHLA from PureProtein (200 μL of a 0.3125 μg/mL solution) to multiple streptavidin (SA) coated disponible sensors of the BLI instrument, Octet RED96 system (FortéBio, Pall Inc., US). Each sHLA immobilized sensor was then dipped for 180 seconds into assay buffer (PBS + 0.05% Tween, GE Healthcare, # 28–995084) to reach a stable baseline. The binding reactions were performed by sequentially dipping the sensors for 1000 s in a row of wells representing increasing concentrations of the investigated soluble mAb (titration representing 3-fold dilution steps: 0, 1.2, 3.7, 11, 33, 100 nM; 200 μL). Subsequently, the sensors were placed into assay buffer for 1800 seconds to record the dissociation. All experiments were carried out at 25°C and at constant plate rotation of 1000 rpm. Raw kinetic data was analyzed using a double reference subtraction approach where the background signal (buffer) was subtracted, using the BLI Data Analysis Software v8.2.07. The binding kinetic profile (k$_a$, k$_d$ and K$_D$) was evaluated using the 1:1 binding model. Affinity determination was realized based on at least two independent experiments. A typical BLI-sensorgram is shown in Figure 1D.

2.3.3 | SPR-assay

Like BLI, SPR is a real-time measurement technique. The ligand (here biotinylated sHLA) must be immobilized to

the renewable streptavidin-modified CAP on a chip. White light is shone onto the chip, and the different solutions consisting of variable analyte (here mAb) concentrations are injected over the surface of the chip. As the antibody binds to the antigen, an alteration of the refractive index (the shift of the resonance angle of the white light) expressed in response units (RU), can be measured. By recording this shift as a function of time, the kinetic events at the surface of the sensor can be visualized in a sensorgram. After the desired association time, buffer is injected on the microfluidics which leads to dissociation of the bound analyte (mAb) and a decrease in SPR signal can be observed.

The setup of the SPR-assay is visualized in Figure 1E. We used the BIAcore instrument 3000 (v4.1.2; GE Healthcare, Uppsala, Sweden). A PBS buffer composed of 10 mM phosphate,137 mM NaCl, and 27 mM KCl with 0.05% Tween20 (w/v), pH 7.4 (GE Healthcare, Uppsala, Sweden, # 28–995084) was used as running buffer to accomplish sHLA immobilization and binding assays. Firstly, for surface conditioning and chip stabilization, three one-min injections of regeneration solution and, subsequently, three complete start-up cycles were performed. Secondly, the biotin reagent CAP (ssDNA-SA, ready-to-use solution) was injected at a flow rate of 2 μL/min for 5 min to build up the renewable streptavidin-modified sensor chip allowing to capture the biotinylated sHLA. Thirdly, biotinylated sHLA proteins (solution with 0.5 μg/mL) were captured (60 seconds) for protein immobilization levels between 40 and 250 RU. Finally, free biotin solution (10 μM in running buffer) was injected once (1 × 1 min) over the sensor surface to block remaining streptavidin binding sites.

All SPR assays were performed at 25°C at flow rates of 5 μL/min (for immobilization) or 50 μL/min (for kinetics), respectively. For all sHLA–mAb interactions, single-cycle kinetics (SCK) were applied. Specifically, five increasing mAb concentrations (12.5, 25, 50, 100, 200 nM) were injected sequentially over the immobilized sHLA at a flow rate of 50 μL/min to prevent the mass transfer effect of protein–protein-interaction (PPI). All samples and blanks were measured in duplicates, with renewal of the sensor surface in between. Regeneration of the chip surface after each analysis cycle was achieved by applying a regeneration solution (6 M Guanidine-HCl in 0.25 M NaOH) at 50 μL/min for 1 min. Data fitting was performed with a 1:1 interaction model using the Biacore 3000 Evaluation v4.1 software. An example of a SPR sensorgram is given in Figure 1F.

2.3.4 | FIDA-assay

Contrarily to the three binding measurement techniques described above, flow-induced dispersion analysis (FIDA) is an immobilization-free ligand binding technique with low interference susceptibility for serum testing. The approach analyses the diffusion behavior of molecular binding partners or emerging complexes under a laminar flow in narrow capillaries.[45] The selective ligand (here sHLA) has to be fluorescently labeled. After injection, the molecules are dispersed in the capillary due to convection and radial diffusion.[35,46] Upon binding of antibody and antigen, their diffusion behavior in the capillary changes, altering their apparent diffusivity D_{app}, determined by means of the fluorescence-peak shape from the ligand (sHLA).[47] Fast diffusion of the indicator (labeled sHLA) in the absence of analyte (antibody) narrows the peak shape, while the peak broadens upon higher concentrations of formed (antibody–antigen) complexes.[48] The degree of complex formation is proportional to the apparent hydrodynamic radius (R_h; nm), which can be calculated on the basis of the peak shape. The applied FIDA setup is visualized in Figure 1G and an example of two fluorescence peak shapes of the indicator is illustrated in the taylorgram of Figure 1H. In this study, FIDA was used to determine DSA affinities of three mAb and for 20 pre-transplant sera of DSA positive patients.

To determine patient DSA-affinity by FIDA, we used the DSA-targeted sHLA and a sHLA representing a self-HLA (preferably an HLA subtype expressed by the same HLA-locus) of the corresponding recipient (negative control) (Table 4). These sHLA were fluorescently labeled (see document S1 for details) and used at a concentration of 100 nM. We serially diluted the appropriate day of transplant serum (10, 5, 2.5, 1.25, 0.625, 0.156, 0.039, 0.0195 and 0.0097% v/v serum) twice, to generate two technical replicates. The titrated samples were incubated for 30 min at room temperature with corresponding sHLA from PureProtein (100 nM; AlexaFluor488-labeled) prior to injection. To assess DSA-concentration, necessary to subsequently determine DSA-affinity, an HLA class specific reference$_{mAb}$ recognizing a conserved binding structure [HLA class I specific: W6/32$_{mAb}$; HLA class II specific: F3.3$_{mAb}$, L243$_{mAb}$ or anti-ZP$_{mAb}$ (Table 2)] was parallely titrated and incubated with the same sHLA. The step-by-step process of the specific measurement concept to reveal DSA-concentration and subsequent DSA-affinity is explained in the supplementary document S1. To calculate half maximum binding from normalized data (R_h-signal translated to % signal) we used the function "one site - specific binding",

$$y = B_{max} * x / (K_D + x)$$

(x = concentration; y = % signal; B_{max} = maximum binding; K_D = DSA-concentration that binds to half of binding sites on HLA at equilibrium)

Details of the applied FIDA-approach are provided in document S1.

2.4 | Statistical analysis

GraphPad Prism 9.3.1 (Graph Pad, SanDiego, California) was used for curve-fittings and for statistical analysis. Correlation analysis was realized using the Pearson r test.

2.5 | Graphical 3D representation of HLA molecules

X-ray crystallographic data from files of the Protein Data Bank (www.rcsb.org[49]) and PyMOL software version 2.5.2 were used to graphically represent HLA molecules and to measure spatial distances between individual amino acids.

3 | RESULTS

3.1 | Affinity determination assay: Technology comparison and their inter-assay precision at known concentration

3.1.1 | HLA-A*02:01 – mouse$_{mAb}$ model

Comparison of various technologies requires the usage of a fixed and defined assay environment to generate useful results. In this model, we decided to apply HLA-A*02:01 in combination with W6/32$_{mAb}$ at known concentrations. These

two binding partners were selected as HLA-A*02:01 is the most frequently studied HLA, and W6/32$_{mAb}$ is very well established in HLA research. The paratope of W6/32$_{mAb}$ interacts with a public conformational HLA class I epitope whose major functional components are the discontinuous residues of lysine at position 121 (heavy chain) and of arginine at position 3 (beta-2 microglobulin) (Figure 2). To determine the variance of the results, we conducted repeated assays.

The K_D values obtained from BLI, SPR, SAB$_{titr}$ were highly consistent. The minimum and maximum affinity measured differed 10.6-fold. Calculated k_a- and k_d-rates, only assayable by BLI and SPR, matched very closely. Repeated measurements revealed coefficient of variation (CV) values of ≤ 0.20 for all four methods. Measurements performed by FIDA revealed slightly lower binding affinities, as in-solution measurements preferably determine monospecific binding. The results are visualized in Figure 2. They indicate that affinity can be accurately determined with all four methods, using the experimental setups described in the Materials and Methods Chapter and visualized in Figure 1.

3.1.2 | HLA-A*02:01 – human$_{mAb}$ model: Binding profiles of two mAbs representing different affinities

To show that all four binding platforms measure affinity with similar accuracy, we generated binding profiles of two
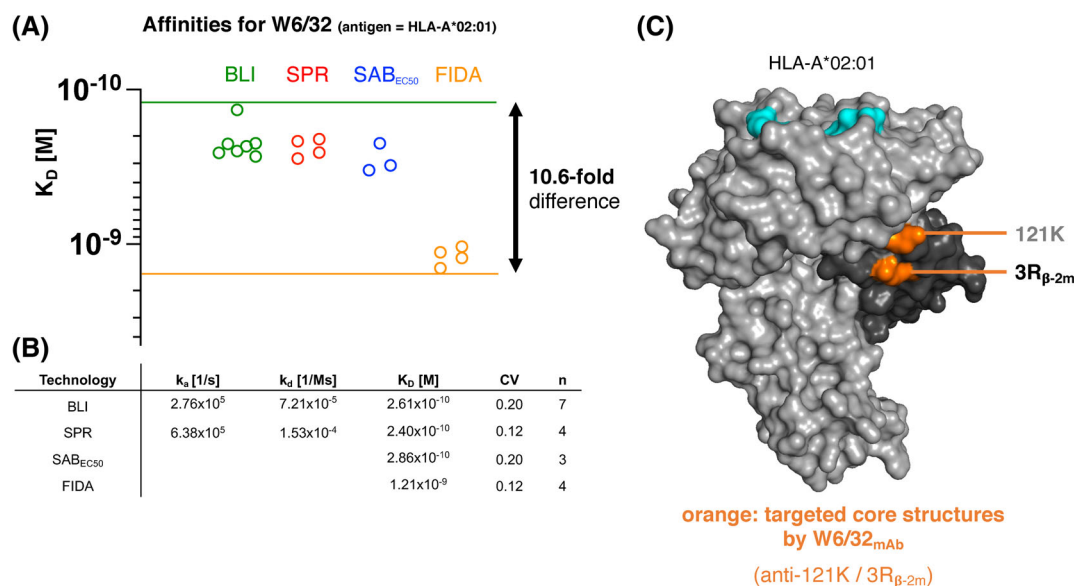
FIGURE 2 Technology dependent affinity results and their inter-assay precision. (A) Affinity results obtained by the indicated technologies. Green line: lowest K_D-value (highest affinity). Orange line: highest K_D-value (lowest affinity). (B) Table with obtained affinity (K_D)-constants, on- and off-rates, and calculated coefficients of variation (CV). (C) Visualization of two core amino acids (orange) targeted by W6/32$_{mAb}$, a lysine at position 121 on the heavy chain (gray) and an arginine at position 3 on the Beta 2-microglobulin (black), shown on HLA-A*02:01 (PDB-ID 5f7d) which was the antigen used for this experiment. (BLI = Bio-Layer Interferometry, FIDA = Flow-induced dispersion analysis, k_a = association rate = on-rate, k_d = dissociation rate = off rate, K_D = dissociation equilibrium constant = affinity, M = Molarity (1 M = 1 mol/L), SAB = Single Antigen Beads, PDB = Protein Data Bank, SPR = Surface Plasmon Resonance)

*HLA-A*02:01* recognizing mAbs with distinguishably different affinities. As such, we investigated SN230G6$_{mAb}$ and SN607D8$_{mAb}$, two antibodies the affinities of which have been published previously,[26,27,29] and differ from each other when interacting with *HLA-A*02:01*. The HLA-antibody SN230G6$_{mAb}$ interacts with eplet 62GE (glycine at position 62 and glutamic acid at position 63), located within the α-helix of the α1-domain shared by other HLA subtypes like HLA-B57 and HLA-B58 (Figure 3). The second mAb, SN607D8$_{mAb}$, recognizes eplet 144TKH (threonine/lysine/histidine at positions 142/144/145), expressed on the opposite lateral side of the molecule, specifically on the α2-helix, also seen on cross-reacting HLA subtypes such as HLA-A68 and HLA-A69 (Figure 3). To compare our results with these earlier findings, we performed affinity measurements by SAB$_{titr}$, BLI and FIDA.

The results indeed confirmed a higher affinity of SN230G6$_{mAb}$ throughout all methods (Figure 3). Looking comparatively at respective on- and off-rates, the obtained SPR- and BLI-data displayed an about 2-fold faster on-rate and more durable (about 2.5-fold lower) off-rate of SN230G6$_{mAb}$ (Table 3). These results demonstrate that previously reported affinity differences between the two mAbs are reproducible.

3.1.3 | Expansion of HLA – human$_{mAb}$ model to other HLA-specific mAbs and other HLA subtypes

To expand the applicability of our technology we tested binding affinities of 12 additional HLA class I-specific reference mAb$_{IgG1}$. Their characteristics are listed in Table 2 and their obtained affinity results in Table 3, together with previously reported affinities[26,27,29,50]). Comparison between solid-phase assay- and in-solution assay-derived results confirmed overall higher K$_D$-values (i.e. lower affinity) obtained with immobilization-free binding technologies such as FIDA and MDS/MAAP. Most affinities were determined using SAB$_{titr}$ (Figure 4). Obtained SAB$_{titr}$-affinity values were distributed over more than two orders of magnitude (0.0276 to 8.37 nM; 303-fold variation). All antibody binding curves demonstrated a sigmoidal shape (exemplarily selection in Figure 4A). For comparative purposes, 11 mAbs were incubated with up to three alternative HLAs expressing the relevant functional epitope. While in 8/11 cases, resulting affinities remained within the same magnitude, BRO11F6$_{mAb}$, MUL4C8$_{mAb}$ and OUW4F11$_{mAb}$ indicated higher inter-molecule binding strength variabilities. Comparing the binding strength between the tested mAb and the immunizing HLA or a
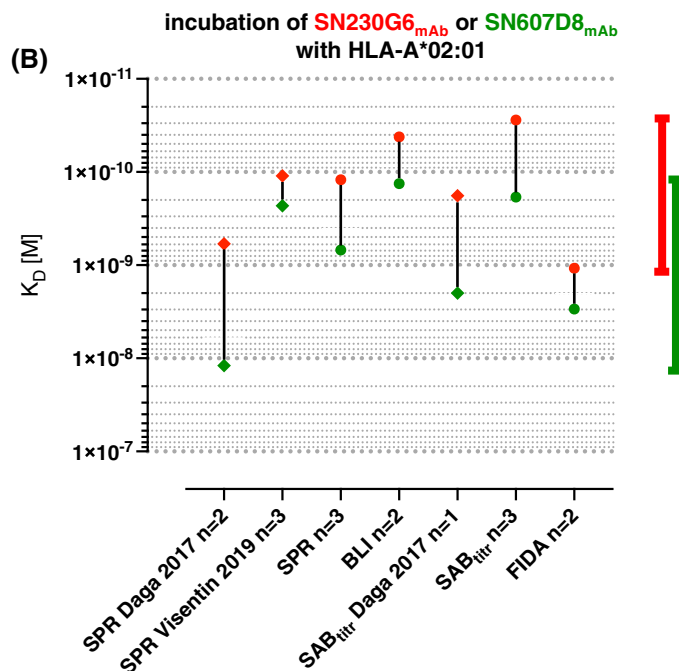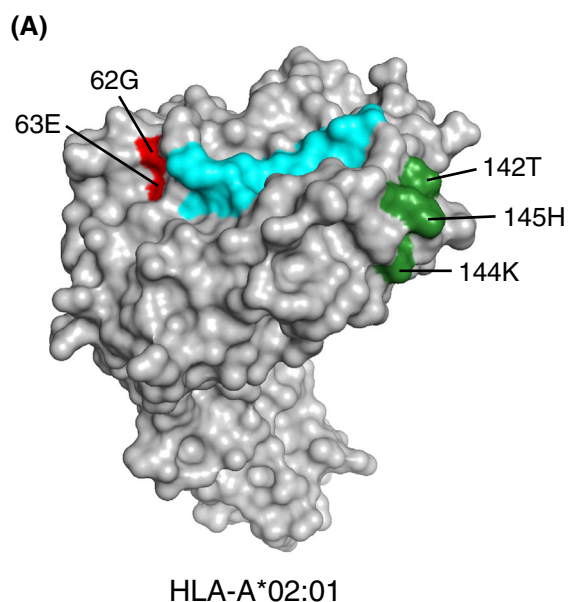

FIGURE 3 Binding profiles of two mAb representing different affinities. (A) Tertiary structure of *HLA-A*02:01* (PDB-ID 5f7d) (heavy chain in gray, peptide in cyan, B2m hidden on the opposite of the molecule), with highlighted amino acids of the targeted eplet that interact with SN230G6$_{mAb}$ (red; 62G + 63E) or SN607D8$_{mAb}$ (green; 142 T + 144 K + 145H). (B) Obtained affinity results. Previously published results: squares. Study-related results: circles. Red: SN230G6$_{mAb}$. Green: SN607D8$_{mAb}$. (B2m = Beta 2-microglobulin, BLI = Bio-Layer Interferometry, E = Glutamic acid, FIDA = Flow-induced dispersion analysis, G = Glycine, H = Histidine, K = Lysine, K$_D$ = dissociation equilibrium constant = affinity, M = Molarity (1 M = 1 mol/L), PDB = Protein Data Bank, SAB = Single Antigen Beads, SPR = Surface Plasmon Resonance, T = Threonine)

TABLE 3 Affinity results of tested HLA-specific monoclonal antibodies

mAb	Ab clone_Isotype/ Subclass_format	tested HLA	Method	Study	n	on rate; k_a	on rate; k_d	K_D [M], average from replicates	K_D [M], calculated from averaged k_d/k_a
1	w6/32_IgG1_hs	A*02:01	BLI	Basel	7	2.76E+05	7.21E-05	**6.75E-10**	2.61E-10
	w6/32_IgG1_hs	A*02:01	SPR	Basel	4	6.38E+05	1.53E-04	**2.40E-10**	2.40E-10
	w6/32_IgG1_hs	A*02:01	FIDA	Basel	4	-	-	**1.21E-09**	
	w6/32_IgG1_hs	A*02:01	SAB$_{titr}$	Basel	3	-	-	**2.88E-10**	
	w6/32_IgG1_hs	A*02:01	SPR	Visentin 2016	2	1.40E+06	9.80E-05	**7.00E-11**	7.00E-11
	w6/32_IgG1_hs	A*03:01	MDS/MAAP	Schneider 2023	3	-	-	**7.00E-10**	
	w6/32_IgG1_hs	A*11:01	SPR	Visentin 2016	2	1.70E+06	1.30E-04	**7.50E-11**	7.65E-11
	w6/32_IgG1_hs	A*11:01	SAB$_{titr}$	Basel	5			**3.39E-10**	
	w6/32_IgG1_hs	B*44:02	SPR	Visentin 2016	2	2.20E+06	1.60E-04	**7.10E-11**	7.27E-11
2	SN230G6_IgG1_hs	A*01:01 (negative control)	BLI	Basel	1	-	-	no binding	
	SN230G6_IgG1_hs	*A*02:01*	BLI	Basel	2	5.93E+05	2.49E-05	**4.32E-11**	4.20E-11
	SN230G6_IgG1_hs	*A*02:01*	BLI	Schneider 2023	1	-	-	**5.60E-09**	
	SN230G6_IgG1_hs	*A*02:01*	SPR	Basel	4	1.34E+06	1.63E-04	**1.21E-10**	1.21E-10
	SN230G6_IgG1_hs	*A*02:01*	SPR	Visentin 2019	3	3.50E+06	3.70E-04	**1.06E-10**	1.06E-10
	SN230G6_IgG1_hs	*A*02:01*	SPR	Daga 2017	2	2.14E+06	1.26E-03	**5.86E-10**	5.86E-10
	SN230G6_IgG1_hs	*A*02:01*	FIDA	Basel	2	-	-	**1.08E-09**	
	SN230G6_IgG1_hs	*A*02:01*	SAB$_{titr}$	Basel	3	-	-	**2.76E-11**	
	SN230G6_IgG1_hs	*A*02:01*	SAB$_{titr}$	Daga 2017	1	-	-	**1.80E-10**	
	SN230G6_IgG1_hs	*A*02:01*	MDS/MAAP	Schneider 2023	1	-	-	**4.80E-09**	
	SN230G6_IgG1_hs	*B*57:01*	BLI	Basel	2	8.91E+05	3.87E-05	**4.36E-11**	4.34E-11
	SN230G6_IgG1_hs	*B*57:01*	SPR	Daga 2017	2	2.43E+06	1.83E-03	**7.53E-10**	7.53E-10
	SN230G6_IgG1_hs	*B*57:01*	SAB$_{titr}$	Daga 2017	1	-	-	**1.50E-10**	
3	SN607D8_IgG1_hs	A*01:01 negative control	BLI	Basel	1	-	-	no binding	
	SN607D8_IgG1_hs	*A*02:01*	BLI	Basel	2	2.75E+05	3.67E-05	**1.38E-10**	1.33E-10
	SN607D8_IgG1_hs	*A*02:01*	SPR	Basel	3	7.95E+05	5.48E-04	**6.92E-10**	6.89E-10
	SN607D8_IgG1_hs	*A*02:01*	SPR	Visentin 2019	3	7.00E+05	1.60E-04	**2.30E-10**	2.29E-10
	SN607D8_IgG1_hs	*A*02:01*	SPR	Daga 2017	2	4.33E+05	5.25E-03	**1.21E-08**	1.21E-08
	SN607D8_IgG1_hs	*A*02:01*	FIDA	Basel	2	-	-	**2.96E-09**	
	SN607D8_IgG1_hs	*A*02:01*	SAB$_{titr}$	Basel	3	-	-	**1.86E-10**	
	SN607D8_IgG1_hs	*A*02:01*	SAB$_{titr}$	Daga 2017	1	-	-	**2.00E-09**	
	SN607D8_IgG1_hs	A*68:01	BLI	Basel	2	1.68E+06	4.49E-05	**2.65E-11**	2.68E-11
	SN607D8_IgG1_hs	A*68:01	SAB$_{titr}$	Daga 2017	1	-	-	**1.60E-09**	
	SN607D8_IgG1_hs	A*68:01	SPR	Daga 2017	2	3.64E+05	1.09E-02	**3.00E-08**	3.00E-08
4	WK1D12_IgG1_hs	A*01:01 negative control	BLI	Basel	1	-	-	no binding	
	WK1D12_IgG1_hs	B*07:02	BLI	Basel	2	2.86E+05	5.32E-05	**1.86E-10**	1.86E-10
	WK1D12_IgG1_hs	B*07:02	SPR	Daga F552017	2	1.20E+06	3.59E-03	**2.99E-09**	2.99E-09

(Continues)

TABLE 3 (Continued)

mAb	Ab clone_Isotype/ Subclass_format	tested HLA	Method	Study	n	on rate; k_a	on rate; k_d	K_D [M], average from replicates	K_D [M], calculated from averaged k_d/k_a
	WK1D12_IgG1_hs	B*07:02	SAB$_{titr}$	Basel	3			**4.83E-10**	
	WK1D12_IgG1_hs	**B*27:05**	BLI	Basel	2	4.76E+05	5.10E-05	**1.07E-10**	1.07E-10
	WK1D12_IgG1_hs	**B*27:05**	SPR	Daga 2017	2	9.45E+05	9.85E-04	**1.04E-09**	1.04E-09
5	BRO11F6_IgG1_hs	A*01:01	BLI	Basel	2	4.00E+05	3.09E-03	**7.83E-09**	7.73E-09
	BRO11F6_IgG1_hs	A*11:01	BLI	Basel	2	8.79E+05	3.71E-04	**4.21E-10**	4.22E-10
	BRO11F6_IgG1_hs	A*11:01	SPR	Visentin 2019	3	7.70E+06	3.20E-03	**4.20E-10**	4.16E-10
	BRO11F6_IgG1_hs	A*11:01	SAB$_{titr}$	Basel	3	-	-	**8.40E-11**	
	BRO11F6_IgG1_hs	A*68:01 negative control	BLI	Basel	1	-	-	no binding	
6	VTM9A10_IgG1_hs	A*01:01 negative control	BLI	Basel	1	-	-	no binding	
	VTM9A10_IgG1_hs	**B*07:02**	BLI	Basel	2	5.15E+05	2.22E-04	**4.51E-10**	4.31E-10
	VTM9A10_IgG1_hs	**B*07:02**	SAB$_{titr}$	Basel	4	-	-	**2.68E-10**	
	VTM9A10_IgG1_hs	B*15:01 negative control	SAB$_{titr}$	Basel	1	-	-	no binding	
	VTM9A10_IgG1_hs	B*27:05	BLI	Basel	2	8.10E+05	2.22E-04	**2.53E-10**	2.74E-10
	VTM9A10_IgG1_hs	B*27:05	SAB$_{titr}$	Basel	1	-	-	**2.07E-10**	
7	VTM1F11_IgG1_hs	A*01:01 negative control	BLI	Basel	1	-	-	no binding	
	VTM1F11_IgG1_hs	**B*07:02**	BLI	Basel	2	5.50E+05	1.28E-04	**2.33E-10**	2.33E-10
	VTM1F11_IgG1_hs	**B*07:02**	SAB$_{titr}$	Basel	4	-	-	**4.23E-10**	
	VTM1F11_IgG1_hs	B*27:05	BLI	Basel	2	7.59E+05	5.77E-04	**7.61E-10**	7.60E-10
8	VTM4D9_IgG1_hs	**B*07:02**	BLI	Basel	1	2.78E+06	3.27E-04	**1.18E-10**	1.18E-10
	VTM4D9_IgG1_hs	**B*07:02**	SAB$_{titr}$	Basel	3	-	-	**7.93E-11**	
	VTM4D9_IgG1_hs	B*27:05	BLI	Basel	1	4.58E+06	5.05E-04	**1.10E-10**	1.10E-10
	VTM4D9_IgG1_hs	B*44:02 negative contol	BLI	Basel	1	-	-	no binding	
9	MUL4C8_IgG1_hs	A*01:01	BLI	Basel	1	1.47E+05	9.15E-03	**6.22E-08**	6.22E-08
	MUL4C8_IgG1_hs	A*01:01	SAB$_{titr}$	Basel	1	-	-	low affinity (no saturation)	
	MUL4C8_IgG1_hs	**A*11:01**	BLI	Basel	1	1.49E+06	2.63E-04	**1.77E-10**	1.77E-10
	MUL4C8_IgG1_hs	**A*11:01**	SAB$_{titr}$	Basel	3	-	-	**6.68E-11**	
	MUL4C8_IgG1_hs	A*68:01 negative control	BLI	Basel	1	-	-	no binding	
	MUL4C8_IgG1_hs	A*68:01 negative control	SAB$_{titr}$	Basel	1	-	-	no binding	
10	BOY2A7_IgG1_hs	A*02:01 negative control	BLI	Basel	1	-	-	no binding	
	BOY2A7_IgG1_hs	A*11:01	SAB$_{titr}$	Basel	3	-	-	**2.31E-10**	
11	WIM8E5_IgG1_hs	A*01:01	BLI	Basel	1	1.48E+06	3.88E-04	**2.62E-10**	2.62E-10
	WIM8E5_IgG2_rc	A*01:01	BLI	Basel	1	1.03E+06	5.00E-04	**4.85E-10**	4.85E-10

TABLE 3   (Continued)

mAb	Ab clone_Isotype/ Subclass_format	tested HLA	Method	Study	n	on rate; k_a	on rate; k_d	K_D [M], average from replicates	K_D [M], calculated from averaged k_d/k_a
	WIM8E5_IgG3_rc	A*01:01	BLI	Basel	1	2.93E+06	2.95E-04	**1.01E-10**	1.01E-10
	WIM8E5_IgG1_hs	A*03:01 negative control	BLI	Basel	1	-	-	no binding	
	WIM8E5_IgG2_rc	A*03:01 negative control	BLI	Basel	1	-	-	no binding	
	WIM8E5_IgG3_rc	A*03:01 negative control	BLI	Basel	1	-	-	no binding	
	WIM8E5_IgG1_hs	A*11:01	SAB$_{titr}$	Basel	3	-	-	**8.47E-11**	
	WIM8E5_IgG2_rc	A*11:01	SAB$_{titr}$	Basel	1	-	-	**3.97E-11**	
	WIM8E5_IgG3_rc	A*11:01	SAB$_{titr}$	Basel	1	-	-	**5.75E-11**	
12	OUW4F11_IgG1_hs	B*07:02	BLI	Basel	1	4.81E+06	4.14E-04	**8.61E-11**	8.61E-11
	OUW4F11_IgG1_hs	B*07:02	SAB$_{titr}$	Basel	2	-	-	**8.37E-09**	
	OUW4F11_IgG1_hs	*B*08:01*	BLI	Basel	1	2.49E+06	2.92E-04	**1.17E-10**	1.17E-10
	OUW4F11_IgG1_hs	*B*08:01*	BLI	Schneider 2023	1			**3.15E-07**	
	OUW4F11_IgG1_hs	*B*08:01*	MDS/MAAP	Schneider 2023	3	-	-	**8.90E-08**	
	OUW4F11_IgG1_hs	B*27:05 negative control	BLI	Basel	1	-	-	no binding	
	OUW4F11_IgG1_hs	B*27:05 negative control	SAB$_{titr}$	Basel	1	-	-	no binding	
	OUW4F11_IgG1_hs	B*35:01	BLI	Basel	1	3.77E+05	8.85E-03	**2.35E-08**	2.35E-08
13	MUL2C6_IgG1_hs	*A*11:01*	SAB$_{titr}$	Basel	3	-	-	**6.74E-11**	
14	VIN1B10_IgG1_hs	A*11:01	SAB$_{titr}$	Basel	2	-	-	**8.26E-11**	
15	F3.3_IgG1_dl-PE	DRB1*07:01	SAB$_{titr}$	Basel	3			**3.38E-10**	
16	SN66E3_IgM_hs	*A*02:01*	SAB$_{titr}$	Basel	2			**2.72E-09**	

Note: hs, hybridoma supernatant; rc, recombinant; dl_PE, dissolved liophylisate, PE labeled; BLI, Bio-Layer Interferometry; FIDA, Flow Induced Dispersion Analysis; MAAP, Microfluidic Antibody Affinity Profiling; MDS, Microfluidic Diffusional Sizing; SAB, Single Antigen Beads.

cross-reactive HLA revealed that measured affinities were either very similar or significantly higher towards the immunizing HLA (Table 3). We also performed negative control experiments consisting of incubations of certain mAb with HLA types not expressing the targeted functional epitope. These assessments revealed either no or only very weak binding (data not shown).

3.1.4 | Antibody mixtures: Impact of spatial distance between antibody targeted epitopes using the *HLA-A*02:01* – human$_{mAb}$ model

DSA is a polyclonal antibody mixture. The result of a DSA-affinity measurement thus reveals a *net* affinity. To demonstrate the impact of more complex antibody mixtures, simulating the polyclonal nature of DSA, we performed two similar experiments where we mixed two HLA-specific mAbs, an IgG1 of high affinity, and an IgM with a fairly low affinity. In the first experiment, both antibodies targeted a functional epitope in a rather spatial distance (situation 1), while in the second experiment each of them targeted a functional epitope in very close spatial proximity (situation 2). We simultaneously incubated the IgG1 antibody (always applying the same molar concentration) with 4 different concentrations of the IgM antibody in the presence of SAB$_{HLA-A*02:01}$ to reveal i) equal molarity, ii) K_D-adjusted molarity (fold molar excess of IgM was (K_D IgM divided by K_D IgG) and 10-fold K_D-adjusted molarity [fold molar excess of IgM was 10-times (K_D IgM divided by K_D IgG)]. Using an IgG- and an IgM-specific fluorochrome-conjugated reporter antibody enabled us to separately monitor the binding behavior of each mAb. As most DSA
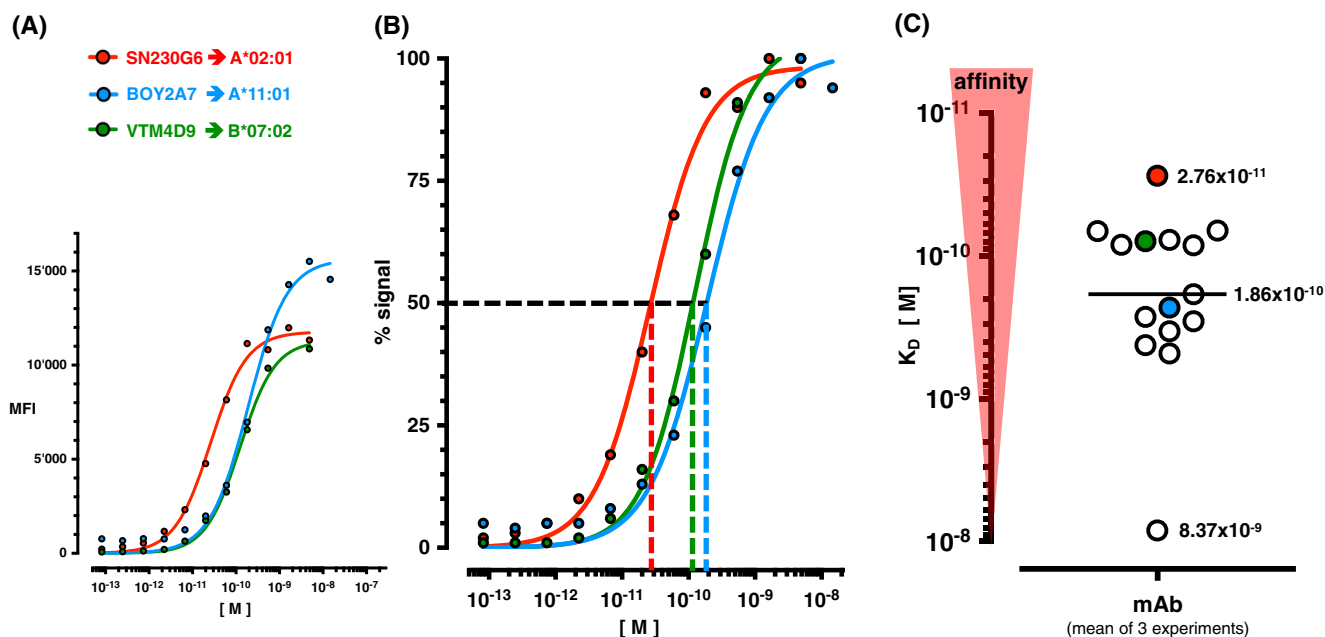
FIGURE 4 Affinity of HLA-specific reference mAbs determined by SAB_{titr}. (A) Antibody binding curves of 3 chosen HLA-specific reference mAbs (all IgG1): red = SN230G6 after reaction with $SAB_{HLA-A*02:01}$, blue = BOY2A7 after reaction with $SAB_{HLA-A*11:01}$, green = VTM4D9 after reaction with $SAB_{HLA-B*07:02}$. X-axis: molarity. Y-axis: NCB corrected trimmed MFI. Applied curve fitting model: "specific binding with hill slope". (B) Antibody binding curves of the same 3 mAbs (colored lines correspond to the mAbs described in A) after normalization of the MFI signal to % signal [100% signal = calculated maximum from the fitting model "specific binding with hill slope"]). Dashed black horizontal line = 50% binding. Dashed colored vertical lines are starting at the inflection point of the corresponding sigmoidal curve and are crossing the x-axis at the concentration representing half maximum binding. (C) Distribution of SAB_{titr} determined affinity results from all HLA-specific mAb_{IgG1} (Table 2), using PE-conjugated anti-IgGpan as reporter-antibody. Y-axis: K_D-values. The width of the red elongated triangle reflects the strengths of the affinity. The dots representing the final result of the corresponding mAbs (A and B) are indicated with the respective color. Minimum, maximum and median (black line) are indicated with the respective numeric K_D-value. (mAb = monoclonal antibody, IgG = Immunoglobulin G, MFI = Mean fluorescence intensity, NCB = Negative control beads, PE = Phycoerythrin, SAB = Single Antigen Beads)

characterization assays focus on DSA_{IgG}, we show the results for IgG.

For situation 1, SN230G6 (IgG1) interacting with eplet 62GE[51] was co-incubated with $SN66E3_{mAb}$ (IgM) interacting with eplet 145KHA.[51] Their previously determined SAB_{titr}-affinity with *HLA-A*02:01* actually differed 98.6-fold ($SN230G6_{mAb}$: $K_D = 0.0276$ nM; $n = 3$; $SN66E3_{mAb}$: $K_D = 2.722$ nM; $n = 2$). The measured spatial distance between the two functional epitopes is 29 Å, suggesting a non-competing binding situation, as the two involved structurally epitopes scarcely overlap.[52] Due to the large size and the multi-valency binding of the involved IgM antibody, steric hindrance is in any case to be expected. Indeed, using an IgG-specific reporter antibody, our measurements revealed a certain decrease of IgG binding proportional to increased amounts of present IgM antibody (Figure 5A). However, the impact of the second antibody was far less pronounced compared to situation 2 with mixtures of $SN607D8_{mAb}$ (IgG) and $SN66E3_{mAb}$ (IgM), both interacting with clearly overlapping eplet configurations (144TKH and 145KHA are located within the same surface exposed region: two of the three AA are

targeted by both mAbs (144 K and 145H).[51,53,54] It can be assumed that upon co-incubation, these two antibodies are competing for the binding sites. Their pre-determined individual binding-affinity to *HLA-A*02:01* was shown to differ 14.6-fold by SAB_{titr} ($SN66E3_{mAb}$: 2.722 nM, $n = 2$; $SN607D8_{mAb}$: 0.1864 nM, $n = 3$). By recording the $SN607D8_{mAb}$ (IgG), again using an IgG-specific secondary antibody, we observed an obvious flattening of the IgG binding curve with increasing amounts of competing $SN66E3_{mAb}$ (IgM) present (Figure 5B). These results imply that binding intensity of co-existing antibodies is mutually impacted by the spatial distance between the targeted structures, as is applicable to DSA mixtures.

3.1.5 | From HLA mAbs to DSA: Determination of concentration and affinity of DSA from serum samples using the FIDA approach

In contrast to mAbs, serum samples from sensitized patients consist almost exclusively of a mixture of HLA-antibodies
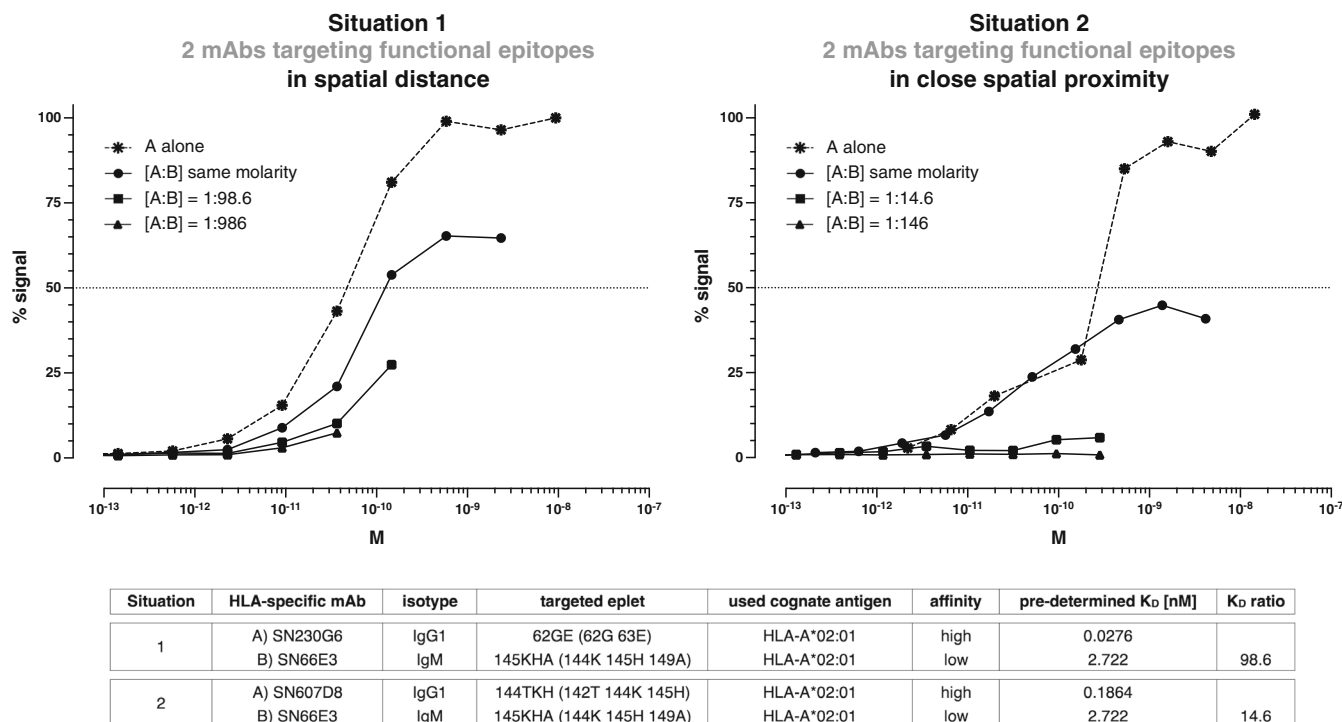
Situation	HLA-specific mAb	isotype	targeted eplet	used cognate antigen	affinity	pre-determined K_D [nM]	K_D ratio
1	A) SN230G6	IgG1	62GE (62G 63E)	HLA-A*02:01	high	0.0276	
	B) SN66E3	IgM	145KHA (144K 145H 149A)	HLA-A*02:01	low	2.722	98.6
2	A) SN607D8	IgG1	144TKH (142T 144K 145H)	HLA-A*02:01	high	0.1864	
	B) SN66E3	IgM	145KHA (144K 145H 149A)	HLA-A*02:01	low	2.722	14.6

FIGURE 5 Impact on mAb binding by co-incubated additional mAb targeting an overlapping eplet or a different eplet in adjacent region. The two mAbs described in the table at the bottom of the figure were co-incubated for 30 minutes with *HLA-A*02:01*. Plotted curves are showing the resulting IgG binding (impacted by the IgM antibody), using PE-conjugated anti-human IgG as reporter antibody. X-axis: molarity. Y-axis: normalized % signal. Three concentration-mixtures were tested: both mAb at equal molarity, mAb$_{IgM}$ concentration equilibrated for affinity-difference, and mAb$_{IgM}$ concentration 10-fold increased. (IgG = Immunoglobulin G, IgM = Immunoglobulin M, M = Molarity (1 M = 1 mol/L), mAb = monoclonal antibody, PE = Phycoerythrin)

from different clones and various Ig-isotypes/subclasses. The investigated 20 DSA probes were taken at the day of transplant from kidney recipients transplanted across the indicated DSA (directed against one mismatch only) (Table 4). They interact with up to five different eplets, as can be seen in Table 4 and Figure 6. Importantly, all sera revealed a negative donor T- and/or B-cell complement-dependent cytotoxicity (CDC) cross-match assay result. Their IgG signal in the original SAB$_{multi}$ test ranged between 571–14,899 MFI. DSA from 8/20 sera (40%) revealed a positive C3d test result, and overall, the C3d-fixation rate correlated with the standard SAB MFI signal. Notably, IgG1 was the predominant subclass (present in all but one serum). Five of the 20 sera (25%) additionally contained DSA$_{IgM}$ and one serum (5%) DSA$_{IgA}$.

The respective sera were incubated with the corresponding cognate sHLA and, using the FIDA approach described in the Materials and Methods-Chapter, investigated for DSA-concentration and subsequently DSA-affinity.

Revealed DSA-concentrations ranged between 1.68 and 184 μg/mL (11.2 and 1223 nM). Having measured also the total immunoglobulin concentrations of the same serum samples allowed us to calculate the proportion of DSA present in the circulation (IgG) within IgG antibodies. The percentage of DSA consisted between 0.024% and 4.9% (Table 4). In 13/20 (65%) patient serum samples, DSA accounted for more than 0.1% of total serum antibodies and 4/20 (25%) sera revealed a proportion of DSA even higher than 1%.

On the basis of the established DSA-concentrations, DSA-affinities were determined. The median of K$_D$s obtained was 5.34 nM, with individual values ranging between 0.055 and 24.7 nM (449-fold variation). The vast majority of apparent DSA-affinity values (18/20 = 90%) was within the range of one order of magnitude. Considering the described technology-dependent affinity-results described in the «*HLA-A*02:01* – mouse$_{mAb}$ model», patient DSA represent relatively high affinities, comparable to those assessed for HLA-specific mAbs. A correlation analysis of the two measures "DSA-concentration" and "DSA-affinity", applying Pearson r correlation, revealed that DSA-affinity is inversely associated with DSA-concentration ($r = 0.486$; $p = 0.03$) (Figure 7). C3d-binding neither associated with DSA-concentration, nor with DSA-affinity, in this data set.

TABLE 4 Characteristics and results of examined DSA

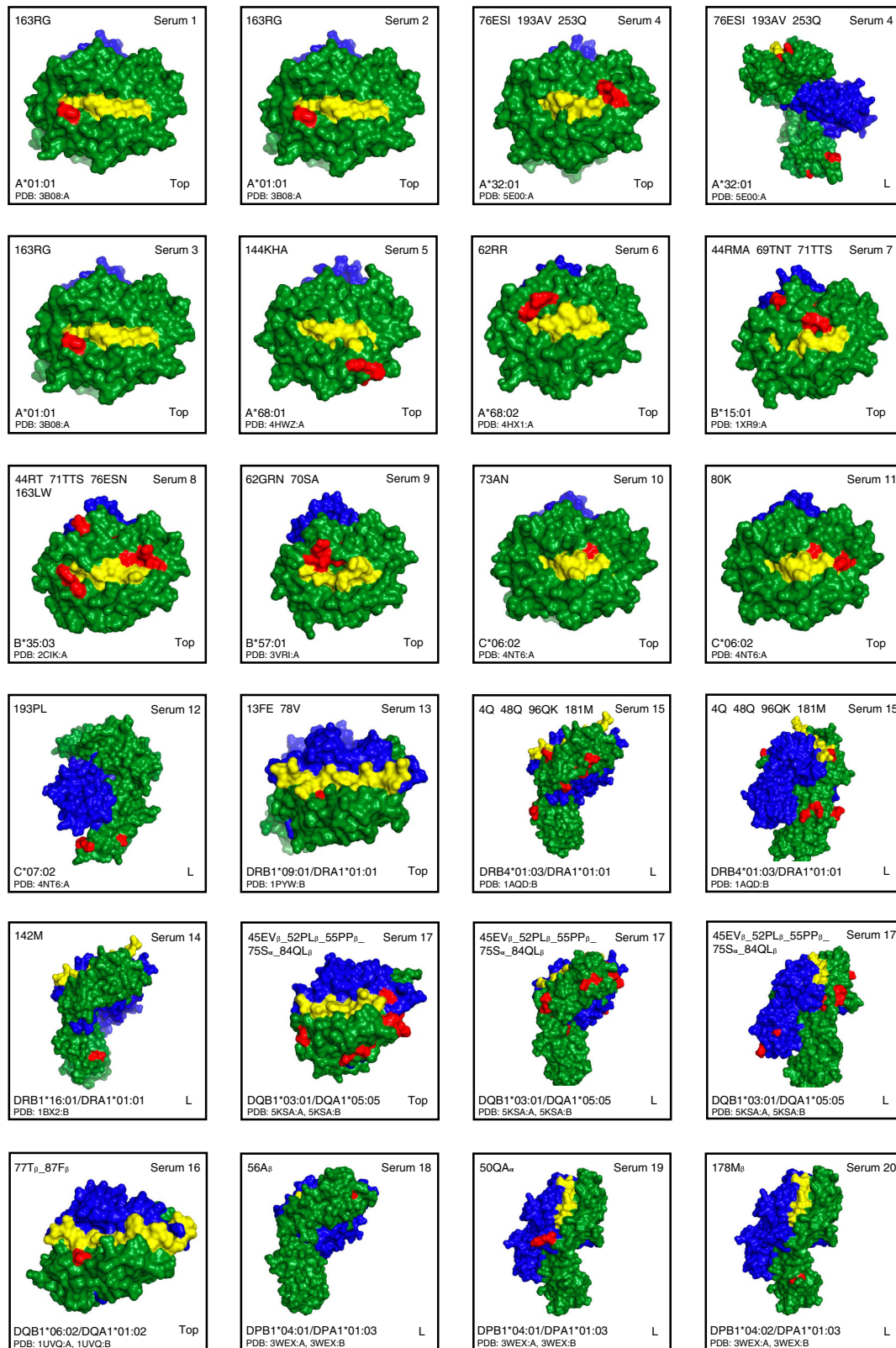| DSA serumID	DSA composition IgG1234 IgM (M) IgA (A)	DSA HLA-specificity	DSA eplet-specificity (antibody verified eplets)	DSA eplet-specificity details	SAB$_{multi}$ MFI	SAB$_{mono}$ MFI	C3d-binding fold over cutoff (>1 = positive)	total IgG [g/L]	FIDA tested mismatched sHLA	FIDA tested self-HLA	reference mAb used	DSA conc by FIDA [µg/mL]	DSA conc by FIDA [nM]	DSA affinity by FIDA KD-value [nM]	% DSA within total IgG
1	1	A*01:01	163RG	163R + 167G	571	1360	0.94	6.86	A*01:01	A*02:01	W6/32	8.19	54.6	**2.87**	0.12
2	1	A*01:01	163RG	163R + 167G	1714	1183	0.60	11.24	A*01:01	A*02:01	W6/32	4.42	29.5	**3.65**	0.04
3	1	A*01:01	163R 163RG	163R, 163R + 167G	3102	5535	1.43	9.09	A*01:01	C*04:01	W6/32	6.74	44.9	**3.02**	0.07
4	1/3/4/M	A*32:01	76ESI 193AV 253Q	76E + 77S + 80I, 193A + 194V, 253Q	4990	11,796	0.28	10.58	A*32:01	A*03:01	W6/32	15.4	102.4	**5.33**	0.15
5	1	A*68:01	144KHA	144 K + 145H + 149A	927	2143	0.92	8.80	A*68:01	A*11:01	W6/32	7.72	51.5	**4.13**	0.09
6	1/2	A*68:02	62RR	62G + 65R	1617	13,195	1.64	7.07	A*68:02	A*02:01	W6/32	5.58	37.2	**4.9**	0.08
7	1/2/3	B*15:01	44RMA 69TNT 71TTS	44R + 45 M + 46A, 69T + 70 N + 71T, 71T + 73 T + 77S	2416	14,457	0.67	9.07	B*15:01	A*02:01	W6/32	20.7	138.0	**12.5**	0.23
8	1	B*35:03	44RT 71TTS 76ESN 163LW	44R + 45 T, 71T + 73 T + 77S, 76E + 77S + 80 N, 163L + 167 W	1810	6816	0.44	4.14	B*35:01	A*02:01	W6/32	6.32	42.2	**5.87**	0.15
9	1/A	B*57:01	62GRN 70SA	70S + 71A, 62G + 65R + 66 N	2625	6209	0.66	5.47	B*57:01	B*15:01	W6/32	8.98	59.9	**7.91**	0.16
10	2	C*06:02	73AN	73A + 77 N	3998	3118	0.49	12.90	C*06:02	C*07:02	W6/32	120.38	802.6	**21.2**	0.93
11	1/M	C*06:02	80 K	80 K	2150	2894	0.51	5.90	C*06:02	C*07:02	W6/32	27.59	184.0	**19.3**	0.47
12	1/2/M	C*07:02	193PL	193P + 194L	2381	4255	0.05	6.02	C*07:02	A*02:01	W6/32	15.94	106.2	**2.95**	0.26
13	1	DRB1*09:01 DRA1*01:01	13FE 78 V	13F + 14E, 78 V	5259	5756	1.81	10.99	DRB1*09:01DRA1*01:01	DRB1*04:01DRA1*01:01	L243	3.31	22.1	**0.055**	0.03
14	1	DRB1*16:01 DRA1*01:01	142 M	142 M	704	3367	1.37	9.01	DRB1*16:01DRA1*01:01	DRB1*07:01DRA1*01:01	L243	54.58	363.9	**5.62**	0.61
15	1	DRB4*01:03 DRA1*01:01	4Q 48Q 96QK 181 M	4Q,18 L + 25 W + 26 N + 41 N + 44 L +48Q + 81Y, 96Q + 98 K, 181 M	3183	5573	2.41	8.40	DRB4*01:03DRA1*01:01	DRB1*04:01DRA1*01:01	L243	4.00	26.7	**0.772**	0.05
16	1/M	DQB1*06:02 DQA1*01:02	77T$_{beta}$ 87F$_{beta}$	77 T, 87F	2283	1858	1.07	6.92	DQB1*06:02DQA1*01:02	DRB1*16:01DRA1*01:01	antiZIP	1.68	11.2	**2.63**	0.02
17	1/3/4/M[a]	DQB1*03:01 DQA1*05:05	45EV$_{beta}$ 52PL$_{beta}$ 55PP$_{beta}$ 75S$_{alpha}$ 84QL$_{beta}$	45E + 46 V + 47Y, 52P + 53 L, 55P + 56P, 75S + 156 L + 161E +163S + 175 K, 84Q + 86E +87L + 89 T + 90 T + 125A	14,899	22,083	5.58	6.30	DQB1*03:01DQA1*02:01	DQB1*06:02DQA1*01:02	antiZIP	65.6	437	**22.1**	1.03
18	1/2/3/4	DPB1*04:01 DPA1*01:03	56A$_{beta}$	56A	11,836	3085	0.88	4.08	DPB1*04:01DPA1*01:03	DPB1*04:02DPA1*01:03	F3.3	108.42	723	**11.5**	2.65
19	1	DPB1*04:01 DPA1*01:03	50QA$_{alpha}$	50Q + 51A	1801	2793	0.55	3.72	DPB1*04:01DPA1*01:03	DPB1*04:02DPA1*01:03	F3.3	184	1223	**5.34**	4.94
20	1	DPB1*04:02 DPA1*01:03	178 M (not Ab-verified)	178 M	1462	2859	1.37	5.67	DPB1*04:02DPA1*01:01	DPB1*04:01DPA1*01:03	F3.3	86.0	573	**24.7**	1.52

FIGURE 6 Visualization of DSA-targeted structures on mismatched HLA molecule. Each box represents the mismatched donor-HLA targeted by the corresponding DSA of indicated patient serum. The structures of the targeted eplet(s) are shown in red. Green: heavy chain (HLA class I) or beta-chain (HLA class II). Blue: B2m (HLA class I) or alpha-chain (HLA class II). Yellow: peptide. Inside each box: Top right: Serum identification. Top left: identified targeted eplet(s) (determined using HLAMatchmaker 3.1). Bottom right: orientation (view to the molecule): Top = top-view, L = lateral view. Bottom left: PDB-ID (from pHLA3D database) of shown HLA. (B2m = beta 2-microglobulin, DSA = donor specific antibody, PDB = Protein Data Bank)
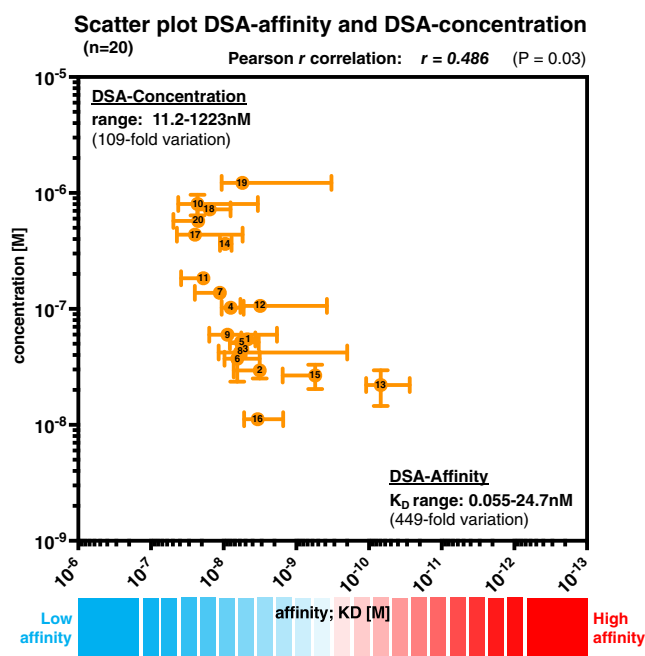
FIGURE 7 Visualization of DSA-affinity and DSA-concentration. Correlation of FIDA determined DSA-affinity and DSA-concentration in the 20 examined pre-transplantation patient serum samples (Pearson's $r = 0.486$; $P = 0.03$). Figure shows mean (orange dot) and the standard deviation (orange error bars) from two experiments for each DSA. Numbers within dots refer to serum number (Table 4). X-axis: net DSA-affinity according to the obtained K_D in mol/L. Y-axis: determined DSA-concentration in mol/L. (K_D = dissociation equilibrium constant = affinity, M = Molarity (1 M = 1 mol/L), DSA = donor specific antibody)

4 | DISCUSSION

Antibody-affinity is a fundamental antibody characteristic and can be determined by a number of biophysical binding measurement platforms. For this study, we first used BLI, SPR, SAB$_{titr}$ and FIDA to assess and compare affinities of well-defined HLA-specific mAbs. The information gained about the binding behavior of the HLA-specific mAbs, which we investigated in the first part of this comparative study, contributes to a more targeted application of these mAbs in the future. We further developed a FIDA assay to determine the affinity of DSA from patient samples, allowing us to herein present, for the first time, DSA binding strengths and their determined variability in a small group of pre-transplant patients.

By using different biophysical binding measurement platforms, technology dependent differences in affinity results must be expected. It is important to recognize that results of affinity measurements can be significantly influenced by whether both molecular binding partners meet in free solution or one partner (e.g. the antigen) is immobilized to a solid phase. Although the latter

approach more accurately represents the investigated real biological situation (i.e. HLA antibody interacting with cellular surface bound HLA molecules), it is susceptible to various interferences (e.g. steric hindrance, rebinding effects, complement interference, high-dose hook effect). Our cross-comparison experiments, using the HLA-A*02:01 – mouse$_{mAb}$ model, demonstrated precise and highly consistent results between the three solid-phase assays (BLI, SPR and SAB$_{titr}$), however, an expected slightly decreased binding strength determined by FIDA, confirming preferential measurement of monovalent IgG binding rather than bivalent binding with an in-solution approach (Figure 2). However, since antibody-affinity clearly correlates with antibody avidity,[55] this is not critical in the context of cross-comparison between patients.

Next, by applying the HLA-A*02:01 – human$_{mAb}$ model, we were able to show that despite technology-dependent shifts in the absolute affinity values measured, the relative comparison between the affinities of two antibodies representing different binding strengths is similar for all four technologies (Figure 3). Subsequently, we expanded our HLA-HLA$_{mAb}$ model to additional HLA-specific mAbs and HLA subtypes. The strong signals obtained - in contrast to the negligible binding signals acquired with HLA subtypes not expressing the functional epitope - confirmed that we measured a very specific interaction between the analyzed mAbs and their cognate eplet-positive HLA subtypes. Determined affinities for all investigated HLA-specific mAbs, considering all used binding technologies and including previously published data from the same mAbs, spanned between more than three orders of magnitude (Table 3). Regarding the variance between measured affinities to several HLA subtypes all representing the same functional epitope of interest, we speculate that physicochemical properties of divergent amino acids, slight structural deviations, variations in protein folding and/or quality differences between the immobilized or soluble HLA used may be the cause.[56] In addition, technical factors of the experimental approach (e.g. whether the antigen or antibody was bound to the solid phase) also exert an influence on the final result.

For heterogeneous antibody mixtures, such as those expected in patient sera, it must be assumed that the type and spatial distance of/between the targeted functional epitope of the involved antibodies are critically impacting the resulting net affinity measured, as the hypervariable regions from the present antibodies of different clonal origin can interact with the very same, with similar, or with multiple spatially separated epitope components (Figure 6). In this context, we simulated the two contrasting situations "targeted eplets in far spatial distance" and "targeted eplets in close spatial proximity" by incubating

two different mixtures consisting of two HLA-specific mAbs (each with known eplet specificity and affinity) with their cognate antigen and subsequently studied how the binding curve of one mAb was impacted by the co-existence of the other mAb. These experiments showed a much clearer distinct displacement of the stronger antibody by drastically increasing the dose of the weaker antibody in the specific situation where both mAbs competed for a very similar binding site. In the previously mentioned experiments, the displacer antibody was an IgM. Interestingly, a fourth of our investigated pre-transplant DSA mixtures included DSA_{IgM}.

Immobilization-free (in-solution) assays offer several advantages in assessing antibody affinity. Our established FIDA approach for patient serum DSA evaluation included the determination of DSA-concentration, the prerequisite to subsequently calculate DSA-affinity. Knowing the quantity may be as clinically important as the quality (affinity) of the given DSA. To obtain DSA-concentration, we used a reference mAb. A similar approach was used to determine the concentration of influenza-specific antibodies by Luminex.[57] While such procedure saves costs, we are aware that our final result may be impacted unilaterally, as each reference antibody represents its own affinity and interacts by an alternative mode of action with its cognate epitope. To improve and standardize the method, we intend to integrate an additional titration with at least a second (lower) antigen concentration for future measurements. Indeed, the concentration and affinity measurements of circulating SARS-CoV-2 antibodies from seropositive individuals published very recently used Microfluidic Antibody Affinity Profiling (MAAP) applied high and low ligand concentrations.[30]

Since we even determined the total IgG-concentration within the serum samples examined, our DSA-study also provides information about the proportion of circulating DSA within total circulating IgG (Table 4): in a fifth of the estimated pre-transplant sera, DSA represented more than 1% of all circulating antibodies, while the lowest proportion of DSA measured was 0.024%. However, our DSA isotype characterization showed that about a third of assessed DSA mixtures consisted not only of IgG (Table 4), indicating a limitation of our approach that used an IgG antibody as a reference: affinity results of multi-isotype containing DSA (6 of 20) must therefore be regarded as potentially slightly inaccurate.

Combining DSA-quantity data (concentration) and DSA-quality data (e.g. affinity, epitope-specificity, complement-binding, Fc-mediated effector cell binding) may provide a more comprehensive image of the deleterious potential of pre-existing or de novo DSA. However, higher case numbers will be needed to investigate associations between these parameters and also to explore differences between HLA class I and II directed DSA. In our study, the investigated class II DSA ($n = 8$) had slightly higher MFIs in the standard SAB assay and revealed moderately higher concentrations but similar affinities compared to HLA class I DSA ($n = 12$).

In addition, longitudinal studies of DSA-concentration and DSA-affinity are needed to reveal the dynamics of DSA-quality and DSA-quantity over time. Such data will help clarify, for example, whether MFI change over time is more likely due to a change in overall DSA-concentration or a change in clonal composition that affects overall DSA-affinity.

Thinking biologically, a humoral immune response with low affinity antibodies can be balanced with a respective high antibody concentration (and vice versa). Indeed, our results demonstrate an association between high affinity and low concentration, in line with observations on influenza virus specific antibodies.[58] The absolute serum DSA-levels determined (Table 4 and Figure 7), although presumed to be slightly biased by the unique isotype/subclass composition of individual DSA (Table 4), are comparable with the sparse published HLA antibody concentrations to date ($n = 5$; 6.1 nM, 15.3 nM, 38.7 nM, 60 nM, 68 nM)[29,59] and reasonably comparable to those published for influenza-specific IgG post-vaccination[57] and for SARS-2-CoV-2-specific IgGs.[60]

Can the Luminex platform, available in most HLA laboratories worldwide also serve to determine DSA-affinity? It is first important to mention that the DSA titer only partially reflects antibody affinity, because antibody titer results are also impacted by the concentration of DSA and the competition with different HLA subtypes expressing the same functional epitope. We have demonstrated that in a clean (e.g. in buffer) and standardized (e.g. applying HLA-specific antibody with known concentration) system, antibody affinity determination is straightforward using Luminex SAB. Indeed, SAB_{titr} revealed mAb-affinities absolutely comparable to those obtained by BLI or SPR. Using SAB with immobilized HLA to test antibodies within serum matrix is, however, more challenging,[61] mainly because of the complement interference effect [62] and/or the high dose hook effect (excessively high HLA antibody concentration[19,63,64]). Indeed, in our patient cohort, 19 out of 20 sera revealed MFI signals (i.e. neat serum) below SAB saturation, either due to low DSA-concentration, or the above mentioned effects. However, precise affinity determination of these DSA by SAB would require full-length binding curves. As used SAB_{mono} are currently not distributed by the two SAB vendors, titration analysis applied with SAB_{multi} instead would be associated with high expenses.

Our DSA-affinity data provide a first insight on how DSA may vary with regard to their apparent affinity

among HLA sensitized patients. From a biological point of view, the approximately 500-fold variability between the equilibrium constants assessed for the 20 DSA described herein may appear rather modest. However, co-consideration of the DSA features 'DSA-concentration' and 'DSA eplet-specificity' may be crucial to characterize the overall pathogenicity of pre-existing circulating DSA more holistically. Clearly, the next step to proceed is to determine the clinical relevance of these measures, by performing retrospective studies on larger patient cohorts.

AUTHOR CONTRIBUTIONS

ACKNOWLEDGMENTS

CONFLICT OF INTEREST STATEMENT

RB is Vice President Product and Services at HLA Protein from PureProtein LLC, which produces soluble HLA. The other authors of this manuscript have no conflicts of interest to disclose.

DATA AVAILABILITY STATEMENT

The data that support the findings of this study are available from the corresponding author upon reasonable request.

ETHICS STATEMENT

All retrospective patient sera analyses were performed with approval from the Ethics Committee of Northwestern and Central Switzerland (approval number EKNZ 2015-403).

ORCID

Sabrina Keller https://orcid.org/0000-0002-8976-9208
Cynthia S. M. Kramer https://orcid.org/0000-0003-1350-2336
Suzanne Bezstarosti https://orcid.org/0000-0002-0315-115X
Stefan Schaub https://orcid.org/0000-0002-9170-1341
Gideon Hönger https://orcid.org/0000-0003-1661-2661

REFERENCES

1. Amico P, Hönger G, Mayr M, Steiger J, Hopfer H, Schaub S. Clinical relevance of pretransplant donor-specific HLA antibodies detected by single-antigen flow-beads. *Transplantation*. 2009;87(11):1681-1688.

2. Sellares J et al. Understanding the causes of kidney transplant failure: the dominant role of antibody-mediated rejection and nonadherence. *Am J Transplant*. 2012;12(2):388-399.

3. Nankivell BJ, Alexander SI. Rejection of the kidney allograft. *N Engl J Med*. 2010;363(15):1451-1462.

4. Einecke G, Sis B, Reeve J, et al. Antibody-mediated microcirculation injury is the major cause of late kidney transplant failure. *Am J Transplant*. 2009;9(11):2520-2531.

5. Pober JS, Sessa WC. Evolving functions of endothelial cells in inflammation. *Nat Rev Immunol*. 2007;7(10):803-815.

6. Murata K, Baldwin WM 3rd. Mechanisms of complement activation, C4d deposition, and their contribution to the pathogenesis of antibody-mediated rejection. *Transplant Rev (Orlando)*. 2009;23(3):139-150.

7. Wasowska BA, Lee CY, Halushka MK, Baldwin WM III. New concepts of complement in allorecognition and graft rejection. *Cell Immunol*. 2007;248(1):18-30.

8. Turgeon NA, Kirk AD, Iwakoshi NN. Differential effects of donor-specific alloantibody. *Transplant Rev (Orlando)*. 2009;23(1):25-33.

9. Hirohashi T, Chase CM, Della Pelle P, et al. A novel pathway of chronic allograft rejection mediated by NK cells and alloantibody. *Am J Transplant*. 2012;12(2):313-321.

10. Christen T, Nahrendorf M, Wildgruber M, et al. Molecular imaging of innate immune cell function in transplant rejection. *Circulation*. 2009;119(14):1925-1932.

11. Valenzuela NM, Trinh KR, Mulder A, Morrison SL, Reed EF. Monocyte recruitment by HLA IgG-activated endothelium: the relationship between IgG subclass and FcgammaRIIa polymorphisms. *Am J Transplant*. 2015;15(6):1502-1518.

12. Patel AM, Pancoska C, Mulgaonkar S, Weng FL. Renal transplantation in patients with pre-transplant donor-specific antibodies and negative flow cytometry crossmatches. *Am J Transplant*. 2007;7(10):2371-2377.

13. Gupta A, Iveson V, Varagunam M, Bodger S, Sinnott P, Thuraisingham RC. Pretransplant donor-specific antibodies in cytotoxic negative crossmatch kidney transplants: are they relevant? *Transplantation*. 2008;85(8):1200-1204.

14. van den Berg-Loonen EM, Billen EVA, Voorter CEM, et al. Clinical relevance of pretransplant donor-directed antibodies detected by single antigen beads in highly sensitized renal transplant patients. *Transplantation*. 2008;85(8):1086-1090.

15. Filippone EJ, Farber JL. Humoral immune response and allograft function in kidney transplantation. *Am J Kidney Dis*. 2015;66(2):337-347.

16. Burns JM, Cornell LD, Perry DK, et al. Alloantibody levels and acute humoral rejection early after positive crossmatch kidney transplantation. *Am J Transplant*. 2008;8(12):2684-2694.

17. Bachler K et al. Efficacy of induction therapy with ATG and intravenous immunoglobulins in patients with low-level donor-specific HLA-antibodies. *Am J Transplant*. 2010;10(5):1254-1262.

18. Ziemann M, Altermann W, Angert K, et al. Preformed donor-specific HLA antibodies in living and deceased donor transplantation: a multicenter study. *Clin J Am Soc Nephrol*. 2019;14(7):1056-1066.

19. Tambur AR, Herrera ND, Haarberg KMK, et al. Assessing antibody strength: comparison of MFI, C1q, and titer information. *Am J Transplant*. 2015;15(9):2421-2430.

20. Loupy A, Lefaucheur C, Vernerey D, et al. Complement-binding anti-HLA antibodies and kidney-allograft survival. *N Engl J Med*. 2013;369(13):1215-1226.

21. Honger G et al. Pretransplant IgG subclasses of donor-specific human leukocyte antigen antibodies and development of antibody-mediated rejection. *Transplantation*. 2011;92(1):41-47.

22. Schaub S, Hönger G, Koller MT, Liwski R, Amico P. Determinants of C1q binding in the single antigen bead assay. *Transplantation*. 2014;98(4):387-393.

23. Neri D, Montigiani S, Kirkham PM. Biophysical methods for the determination of antibody-antigen affinities. *Trends Biotechnol*. 1996;14(12):465-470.

24. Myszka DG. Kinetic analysis of macromolecular interactions using surface plasmon resonance biosensors. *Curr Opin Biotechnol*. 1997;8(1):50-57.

25. Papalia GA, Baer M, Luehrsen K, Nordin H, Flynn P, Myszka DG. High-resolution characterization of antibody fragment/antigen interactions using Biacore T100. *Anal Biochem*. 2006;359(1):112-119.

26. Daga S, Moyse H, Briggs D, et al. Direct quantitative measurement of the kinetics of HLA-specific antibody interactions with isolated HLA proteins. *Hum Immunol*. 2018;79(2):122-128.

27. Visentin J, Leu DL, Mulder A, et al. Measuring anti-HLA antibody active concentration and affinity by surface plasmon resonance: comparison with the luminex single antigen flow beads and T-cell flow cytometry crossmatch results. *Mol Immunol*. 2019;108:34-44.

28. Abdiche Y, Malashock D, Pinkerton A, Pons J. Determining kinetics and affinities of protein interactions using a parallel real-time label-free biosensor, the octet. *Anal Biochem*. 2008; 377(2):209-217.

29. Schneider MM, Scheidt T, Priddey AJ. Microfluidic antibody affinity profiling for In-solution characterisation of alloantibody-HLA interactions in human serum. *Biosens Bioelectron*. 2023;228:115196.

30. Schneider MM, Emmenegger M, Xu CK, et al. Microfluidic characterisation reveals broad range of SARS-CoV-2 antibody affinity in human plasma. *Life Sci Alliance*. 2022;5(2): e202101270.

31. El-Awar N, Lee J, Terasaki PI. HLA antibody identification with single antigen beads compared to conventional methods. *Hum Immunol*. 2005;66(9):989-997.

32. Weinstock C, Schnaidt M. The complement-mediated prozone effect in the Luminex single-antigen bead assay and its impact on HLA antibody determination in patient sera. *Int J Immunogenet*. 2013;40(3):171-177.

33. Schwaiger E, Wahrmann M, Bond G, Eskandary F, Böhmig GA. Complement component C3 activation: the leading cause of the prozone phenomenon affecting HLA antibody detection on single-antigen beads. *Transplantation*. 2014; 97(12):1279-1285.

34. Arosio P, Müller T, Rajah L, et al. Microfluidic diffusion analysis of the sizes and interactions of proteins under native solution conditions. *ACS Nano*. 2016;10(1):333-341.

35. Jensen H, Ostergaard J. Flow induced dispersion analysis quantifies noncovalent interactions in nanoliter samples. *J Am Chem Soc*. 2010;132(12):4070-4071.

36. Amit AG, Mariuzza RA, Phillips SEV, Poljak RJ. Three-dimensional structure of an antigen-antibody complex at 2.8 a resolution. *Science*. 1986;233(4765):747-753.

37. Duquesnoy RJ, Mulder A, Askar M, Fernandez-Vina M, Claas FHJ. HLAMatchmaker-based analysis of human monoclonal antibody reactivity demonstrates the importance of an additional contact site for specific recognition of triplet-defined epitopes. *Hum Immunol*. 2005;66(7):749-761.

38. MacCallum RM, Martin AC, Thornton JM. Antibody-antigen interactions: contact analysis and binding site topography. *J Mol Biol*. 1996;262(5):732-745.

39. Buchli R, VanGundy RS, Hickman-Miller HD, Giberson CF, Bardet W, Hildebrand WH. Real-time measurement of in vitro peptide binding to soluble *HLA-A*0201* by fluorescence polarization. *Biochemistry*. 2004;43(46):14852-14863.

40. Pei R, Wang G, Tarsitani C, et al. Simultaneous HLA class I and class II antibodies screening with flow cytometry. *Hum Immunol*. 1998;59(5):313-322.

41. Garcia-Sanchez C, Usenko CY, Herrera ND, Tambur AR. The shared epitope phenomenon-a potential impediment to virtual crossmatch accuracy. *Clin Transplant*. 2020;34(8):e13906.

42. Maguire CH, Schinstock CA, Tambur AR. Measuring human leukocyte antigen alloantibodies: beyond a binary decision. *Curr Opin Organ Transplant*. 2020;25(6):529-535.

43. Bielmann D, Hönger G, Lutz D, Mihatsch MJ, Steiger J, Schaub S. Pretransplant risk assessment in renal allograft recipients using virtual crossmatching. *Am J Transplant*. 2007;7(3): 626-632.

44. Honger G et al. Toward defining the immunogenicity of HLA epitopes: impact of HLA class I eplets on antibody formation during pregnancy. *HLA*. 2020;96(5):589-600.

45. Otzen DE, Buell AK, Jensen H. Microfluidics and the quantification of biomolecular interactions. *Curr Opin Struct Biol*. 2021;70:8-15.

46. Pedersen ME, Ostergaard J, Jensen H. Flow-induced dispersion analysis (FIDA) for protein quantification and characterization. *Methods Mol Biol*. 2019;1972:109-123.

47. Poulsen NN, Andersen NZ, Østergaard J, Zhuang G, Petersen NJ, Jensen H. Flow induced dispersion analysis rapidly quantifies proteins in human plasma samples. *Analyst*. 2015;140(13):4365-4369.

48. Sharma U, Gleason NJ, Carbeck JD. Diffusivity of solutes measured in glass capillaries using Taylor's analysis of dispersion and a commercial CE instrument. *Anal Chem*. 2005;77(3): 806-813.

49. Berman HM, Westbrook J, Feng Z, et al. The protein data Bank. *Nucleic Acids Res*. 2000;28(1):235-242.

50. Visentin J, Minder L, Lee JH, Taupin JL, di Primo C. Calibration free concentration analysis by surface plasmon resonance in a capture mode. *Talanta*. 2016;148:478-485.

51. Bezstarosti S et al. A comprehensive evaluation of the antibody-verified status of Eplets listed in the HLA epitope registry. *Front Immunol*. 2021;12:800946.

52. Marrari M, Mostecki J, Mulder A, Claas F, Balazs I, Duquesnoy RJ. Human monoclonal antibody reactivity with human leukocyte antigen class I epitopes defined by pairs of mismatched eplets and self-eplets. *Transplantation*. 2010; 90(12):1468-1472.

53. Mulder A, Kardol M, Regan J, Buelow R, Claas F. Reactivity of twenty-two cytotoxic human monoclonal HLA antibodies

towards soluble HLA class I in an enzyme-linked immunosorbent assay (PRA-STAT). *Hum Immunol.* 1997;56(1–2):106-113.

54. Mulder A, Eijsink C, Kester MGD, et al. Impact of peptides on the recognition of HLA class I molecules by human HLA antibodies. *J Immunol.* 2005;175(9):5950-5957.

55. Griswold WR. A quantitative relationship between antibody affinity and antibody avidity. *Immunol Invest.* 1987;16(2):97-106.

56. Kramer CSM, Israeli M, Mulder A, et al. The long and winding road towards epitope matching in clinical transplantation. *Transpl Int.* 2019;32(1):16-24.

57. Wang J, Hilchey SP, Hyrien O, et al. Multi-dimensional measurement of antibody-mediated heterosubtypic immunity to influenza. *PLoS One.* 2015;10(6):e0129858.

58. Linnik J, Syedbasha M, Hollenstein Y, Halter J, Egli A, Stelling J. Model-based inference of neutralizing antibody avidities against influenza virus. *PLoS Pathog.* 2022;18(1):e1010243.

59. McMurtrey C, Lowe D, Buchli R, et al. Profiling antibodies to class II HLA in transplant patient sera. *Hum Immunol.* 2014;75(3):261-270.

60. Schneider MM, Emmenegger M, Xu CK, et al. Microfluidic characterisation reveals broad range of SARS-CoV-2 antibody affinity in human plasma. *Life Sci Alliance.* 2021;5(2):e202101270.

61. Lobashevsky AL. Methodological aspects of anti-human leukocyte antigen antibody analysis in solid organ transplantation. *World J Transplant.* 2014;4(3):153-167.

62. Berth M. Complement interference is not the same as a pro-zone phenomenon. *Am J Transplant.* 2016;16(5):1638.

63. Tambur AR, Wiebe C. HLA diagnostics: evaluating DSA strength by titration. *Transplantation.* 2018;102(1S Suppl 1):S23-S30.

64. Tambur AR, Schinstock C, Maguire C, Lowe D, Smith B, Stegall M. Estimating alloantibody levels in highly sensitized renal allograft candidates: using serial dilutions to demonstrate a treatment effect in clinical trials. *Am J Transplant.* 2021;21(3):1278-1284.

SUPPORTING INFORMATION

Additional supporting information can be found online in the Supporting Information section at the end of this article.